



Observation of $\Lambda_b^0 \rightarrow D^+ p \pi^- \pi^-$ and $\Lambda_b^0 \rightarrow D^{*+} p \pi^- \pi^-$ decays

LHCb collaboration[†]

Abstract

The multihadron decays $\Lambda_b^0 \rightarrow D^+ p \pi^- \pi^-$ and $\Lambda_b^0 \rightarrow D^{*+} p \pi^- \pi^-$ are observed in data corresponding to an integrated luminosity of 3 fb^{-1} , collected in proton-proton collisions at centre-of-mass energies of 7 and 8 TeV by the LHCb detector. Using the decay $\Lambda_b^0 \rightarrow \Lambda_c^+ \pi^+ \pi^- \pi^-$ as a normalisation channel, the ratio of branching fractions is measured to be

$$\frac{\mathcal{B}(\Lambda_b^0 \rightarrow D^+ p \pi^- \pi^-)}{\mathcal{B}(\Lambda_b^0 \rightarrow \Lambda_c^+ \pi^+ \pi^- \pi^-)} \times \frac{\mathcal{B}(D^+ \rightarrow K^- \pi^+ \pi^+)}{\mathcal{B}(\Lambda_c^+ \rightarrow p K^- \pi^+)} = (5.35 \pm 0.21 \pm 0.16) \%,$$

where the first uncertainty is statistical and the second systematic. The ratio of branching fractions for the $\Lambda_b^0 \rightarrow D^{*+} p \pi^- \pi^-$ and $\Lambda_b^0 \rightarrow D^+ p \pi^- \pi^-$ decays is found to be

$$\frac{\mathcal{B}(\Lambda_b^0 \rightarrow D^{*+} p \pi^- \pi^-)}{\mathcal{B}(\Lambda_b^0 \rightarrow D^+ p \pi^- \pi^-)} \times (\mathcal{B}(D^{*+} \rightarrow D^+ \pi^0) + \mathcal{B}(D^{*+} \rightarrow D^+ \gamma)) = (61.3 \pm 4.3 \pm 4.0) \%.$$

Submitted to JHEP

© 2024 CERN for the benefit of the LHCb collaboration. CC BY 4.0 licence.

[†]Authors are listed at the end of this paper.

1 Introduction

Nonleptonic decays with multiple hadrons, such as $\Lambda_b^0 \rightarrow D^+ p \pi^- \pi^-$ and $\Lambda_b^0 \rightarrow \Lambda_c^+ \pi^- \pi^+ \pi^-$, are a useful platform for testing non-perturbative quantum chromodynamics (QCD) approaches such as QCD factorisation (QCDF). At the quark level these Λ_b^0 baryon decays are mediated by the weak $b \rightarrow c \bar{c} s$ and $b \rightarrow c \bar{u} d$ transitions.¹ Calculating the rates for these decays is more challenging than for their semileptonic $b \rightarrow c \ell^- \bar{\nu}_\ell$ partners, since strong interactions are present in both the hadronic initial and final states. Despite these difficulties, which are due to QCD effects, substantial progress has been made in computing hadronic two-body and quasi-two-body decays; earlier calculations [1–4] have been refined in Refs. [5, 6]. These theory predictions agree well with both the CDF measurement of Λ_b^0 production and decays [7], and a similar LHCb measurement [8]. Formulated within the framework of QCDF, these predictions are calculated for several decay modes, $\Lambda_b^0 \rightarrow \Lambda_c^+(\pi^-, \rho^-, a_1^-)$, including exclusive modes where the intermediate resonance decays into a final state with multiple pions, *e.g.* $a_1^- \rightarrow \pi^- \pi^- \pi^+$ [5]. Such decay channels contribute to the multihadron $\Lambda_b^0 \rightarrow \Lambda_c^+ \pi^- \pi^+ \pi^-$ decay analysed in this study.

Final state protons and charm mesons are of particular interest in multihadron decays of beauty baryons, where the c -quark from the $b \rightarrow c$ transition hadronises into the final state separate from the baryon, *i.e.* a charm meson and a proton. This topology is not only important for charm baryon and meson spectroscopy, but also sensitive to QCD effects in beauty baryons as well as charm-quark hadronisation. However, this topology has not been widely studied. Currently, only a few decay modes of beauty baryons with the final state configuration described above are known: $\Lambda_b^0 \rightarrow D^0 p \pi^-$ [9–11], $\Lambda_b^0 \rightarrow D^0 p K^-$ and $\Xi_b^0 \rightarrow D^0 p K^-$ [11]. The amplitude analysis of $\Lambda_b^0 \rightarrow D^0 p K^-$ decays discovered a rich resonance structure allowing the study of excited charm baryons [12]. Recently, the LHCb collaboration reported an observation of the $\Lambda_b^0 \rightarrow D p K^-$ channel with a $D \rightarrow K^\mp \pi^\pm$ decay, where the state D is a superposition of D^0 and \bar{D}^0 states [13]. The CP asymmetry in this decay and the ratio of branching fractions for the $\Lambda_b^0 \rightarrow (D \rightarrow K^- \pi^+) p K^-$ and $\Lambda_b^0 \rightarrow (D \rightarrow K^+ \pi^-) p K^-$ decays are also measured.

In this paper, the first observation of the $\Lambda_b^0 \rightarrow D^+ p \pi^- \pi^-$ and $\Lambda_b^0 \rightarrow D^{*+} p \pi^- \pi^-$ multihadron decay modes is reported. The measurements are based on proton-proton (pp) collision data, corresponding to integrated luminosities of 1 and 2 fb⁻¹ collected with the LHCb detector at center-of-mass energies of 7 and 8 TeV, respectively. The following ratios of branching fractions are reported

$$\mathcal{R}_{D^+} \equiv \frac{\mathcal{B}(\Lambda_b^0 \rightarrow D^+ p \pi^- \pi^-)}{\mathcal{B}(\Lambda_b^0 \rightarrow \Lambda_c^+ \pi^+ \pi^- \pi^-)} \times \frac{\mathcal{B}(D^+ \rightarrow K^- \pi^+ \pi^+)}{\mathcal{B}(\Lambda_c^+ \rightarrow p K^- \pi^+)}, \quad (1a)$$

$$\mathcal{R}_{D^{*+}} \equiv \frac{\mathcal{B}(\Lambda_b^0 \rightarrow D^{*+} p \pi^- \pi^-)}{\mathcal{B}(\Lambda_b^0 \rightarrow D^+ p \pi^- \pi^-)} \times \mathcal{B}(D^{*+} \rightarrow D^+ \pi^0 / \gamma), \quad (1b)$$

where $\mathcal{B}(D^{*+} \rightarrow D^+ \pi^0 / \gamma)$ equals $\mathcal{B}(D^{*+} \rightarrow D^+ \pi^0) + \mathcal{B}(D^{*+} \rightarrow D^+ \gamma)$, and the $\Lambda_b^0 \rightarrow \Lambda_c^+ \pi^+ \pi^- \pi^-$ mode with the $\Lambda_c^+ \rightarrow p K^- \pi^+$ decay is used as the normalisation channel. No theory predictions are currently available for the decay modes $\Lambda_b^0 \rightarrow D^+ p \pi^- \pi^-$ and $\Lambda_b^0 \rightarrow D^{*+} p \pi^- \pi^-$.

¹The inclusion of charge-conjugate processes is implied throughout the paper.

2 Detector and simulation

The LHCb detector [14, 15] is a single-arm forward spectrometer covering the pseudorapidity range $2 < \eta < 5$, designed for the study of particles containing b or c quarks. The detector includes a high-precision tracking system consisting of a silicon-strip vertex detector surrounding the pp interaction region, a large-area silicon-strip detector located upstream of a dipole magnet with a bending power of about 4 Tm, and silicon-strip detectors and straw drift tubes placed downstream of the magnet. The tracking system provides a measurement of the momentum, p , of charged particles with a relative uncertainty that varies from 0.5% at low momentum to 1.0% at 200 GeV/ c . The minimum distance of a track to a primary pp collision vertex (PV), the impact parameter (IP), is measured with a resolution of $(15 + 29/p_T) \mu\text{m}$, where p_T is the component of the momentum transverse to the beam, in GeV/ c . Different types of charged hadrons are distinguished using information from two ring-imaging Cherenkov detectors. Photons, electrons and hadrons are identified by a calorimeter system consisting of scintillating-pad and preshower detectors, an electromagnetic and a hadronic calorimeter. Muons are identified by a system composed of alternating layers of iron and multiwire proportional chambers.

The online event selection is performed by a trigger system. The trigger consists of a hardware stage, based on information from the calorimeter and muon systems, followed by a software stage, which applies a full event reconstruction [16]. The events used in this analysis are selected at the hardware stage by requiring a cluster in the calorimeters with transverse energy greater than 3.6 GeV. The software trigger requires a two-, three- or four-track secondary vertex with a large p_T sum of the particles and a significant displacement from the primary pp interaction vertices (PVs). At least one charged particle should have $p_T > 1.7 \text{ GeV}/c$ and large χ_{IP}^2 with respect to any PV, where χ_{IP}^2 is defined as the difference in fit χ^2 of a given PV reconstructed with and without the considered track. A multivariate algorithm is used for the identification of secondary vertices consistent with the decay of a b hadron [17].

Simulated collision events are used to model the effects of the detector acceptance and the imposed selection requirements for signal decay modes. In the simulation, pp collisions are generated using PYTHIA [18] with a specific LHCb configuration [19]. The p_T and rapidity spectra of the Λ_b^0 baryons in simulation are corrected to match those for the reconstructed $\Lambda_b^0 \rightarrow \Lambda_c^+ \pi^+ \pi^- \pi^-$ decays, which constitute a large data sample used for normalisation. Decays of unstable particles are described by EVTGEN [20], in which final-state radiation is generated using PHOTOS [21]. A four-body phase-space decay model is used for the $\Lambda_b^0 \rightarrow D^+ p \pi^- \pi^-$ and $\Lambda_b^0 \rightarrow D^{*+} p \pi^- \pi^-$ decay modes. The decays $\Lambda_b^0 \rightarrow \Lambda_c^+ \pi^+ \pi^- \pi^-$ are simulated as a mixture of decays via intermediate excited $\Sigma_c^{(*)}$ resonances $\Lambda_b^0 \rightarrow (\Sigma_c^{(*)++} \rightarrow \Lambda_c^+ \pi^+) \pi^- \pi^-$ and $\Lambda_b^0 \rightarrow (\Sigma_c^{(*)0} \rightarrow \Lambda_c^+ \pi^-) \pi^+ \pi^-$; excited Λ_c^+ baryons $\Lambda_b^0 \rightarrow (\Lambda_c(2595)^+ \rightarrow \Lambda_c^+ \pi^+ \pi^-) \pi^-$ and $\Lambda_b^0 \rightarrow (\Lambda_c(2625)^+ \rightarrow \Lambda_c^+ \pi^+ \pi^-) \pi^-$; or light unflavoured hadrons $\Lambda_b^0 \rightarrow \Lambda_c^+ a_1^-$, $\Lambda_b^0 \rightarrow \Lambda_c^+ \rho^0 \pi^-$, and $\Lambda_b^0 \rightarrow \Lambda_c^+ f_2(1270) \pi^-$. The decay models are corrected to reproduce the ten two- and three-body mass distributions from the signals observed in data, further described in Sec. 5. The interaction of the generated particles with the detector and its response are implemented using the GEANT4 toolkit [22] as described in Ref. [23]. To account for imperfections in the simulation of charged-particle reconstruction, the track reconstruction efficiency determined from simulation is corrected using control channels in data [24].

3 Event selection

The $\Lambda_b^0 \rightarrow D^+ p \pi^- \pi^-$ and $\Lambda_b^0 \rightarrow \Lambda_c^+ \pi^+ \pi^- \pi^-$ decays are reconstructed using the $D^+ \rightarrow K^- \pi^+ \pi^+$ and $\Lambda_c^+ \rightarrow p K^- \pi^+$ decay channels, respectively. The selection begins with good-quality reconstructed charged tracks that are inconsistent with being produced in a pp interaction vertex. Kaons, pions and protons, identified using information from the RICH detectors [25, 26], are selected from well-reconstructed tracks within the acceptance of the spectrometer with $p_T > 100 \text{ MeV}/c$. To allow for efficient particle identification, kaons and pions are required to have a momentum between 3 and $120 \text{ GeV}/c$, while protons must have momenta between 9 and $120 \text{ GeV}/c$.

The $D^+ \rightarrow K^- \pi^+ \pi^+$ and $\Lambda_c^+ \rightarrow p K^- \pi^+$ candidates are reconstructed from selected kaon, pion and proton candidates requiring $K^- \pi^+ \pi^+$ and $p K^- \pi^+$ combinations to form a good quality three-prong common vertex, which is significantly separated from any PV. A reconstructed mass for the D^+ and Λ_c^+ candidates is required to be within ± 34 and $\pm 24 \text{ MeV}/c^2$ mass windows around the known masses of the D^+ and Λ_c^+ hadrons [27], respectively. These mass ranges correspond to approximately $\pm 4\sigma_m$ regions, where σ_m is the mass resolution. Three-track combinations are also formed of $p \pi^- \pi^-$ and $\pi^+ \pi^- \pi^-$ particle triplets, and are required to have a good-quality common vertex that is distinct from the PV. The mass of these $p \pi^- \pi^-$ and $\pi^+ \pi^- \pi^-$ combinations are required to be below 4 and $3 \text{ GeV}/c^2$, respectively.

The reconstructed D^+ and Λ_c^+ candidates are combined with selected $p \pi^- \pi^-$ and $\pi^- \pi^+ \pi^-$ candidates to form Λ_b^0 candidates. Only Λ_b^0 candidates with a transverse momentum above $3 \text{ GeV}/c$ are selected for further analysis. To improve the mass resolution for the Λ_b^0 candidates, a kinematic fit is performed [28], which constrains the mass of the D^+ and Λ_c^+ hadron candidates to their known masses [27] and requires the Λ_b^0 candidate to originate from its associated PV. A requirement on the χ^2 from this fit further suppresses background. The reconstructed Λ_b^0 decay vertex is required to be distinct from the PV, with the proper decay time of the Λ_b^0 candidate restricted to be above $100 \mu\text{m}/c$. The proper decay time of the D^+ and Λ_c^+ candidates calculated with respect to the reconstructed Λ_b^0 decay vertex is required to be positive within the resolution. These two requirements reduce the background contributions from charmed hadrons produced directly in the pp interaction, and random combinations of tracks forming fake D^+ or Λ_c^+ candidates. At least one track from the selected Λ_b^0 candidate must be matched with a high energy deposit in the calorimeter system, used in the hardware-trigger stage. The mass distributions for selected $\Lambda_b^0 \rightarrow D^+ p \pi^- \pi^-$ and $\Lambda_b^0 \rightarrow \Lambda_c^+ \pi^+ \pi^- \pi^-$ candidates are shown in Figs. 1 and 2, respectively.

4 Signal determination

The $D^+ p \pi^- \pi^-$ mass distribution shown in Fig. 1 exhibits a narrow peak corresponding to the $\Lambda_b^0 \rightarrow D^+ p \pi^- \pi^-$ decay. In addition, a structure around $5.4 - 5.5 \text{ GeV}/c^2$ is visible. This structure corresponds to the $\Lambda_b^0 \rightarrow D^{*+} p \pi^- \pi^-$ decay followed by the decay of the D^{*+} meson into $D^+ \pi^0$ or $D^+ \gamma$ states, where the neutral particle is not reconstructed. An extended unbinned maximum-likelihood fit to the $D^+ p \pi^- \pi^-$ mass distribution is performed using a function consisting of a sum of the four following contributions.

- A $\Lambda_b^0 \rightarrow D^+ p \pi^- \pi^-$ component, parameterised by a modified Gaussian function with

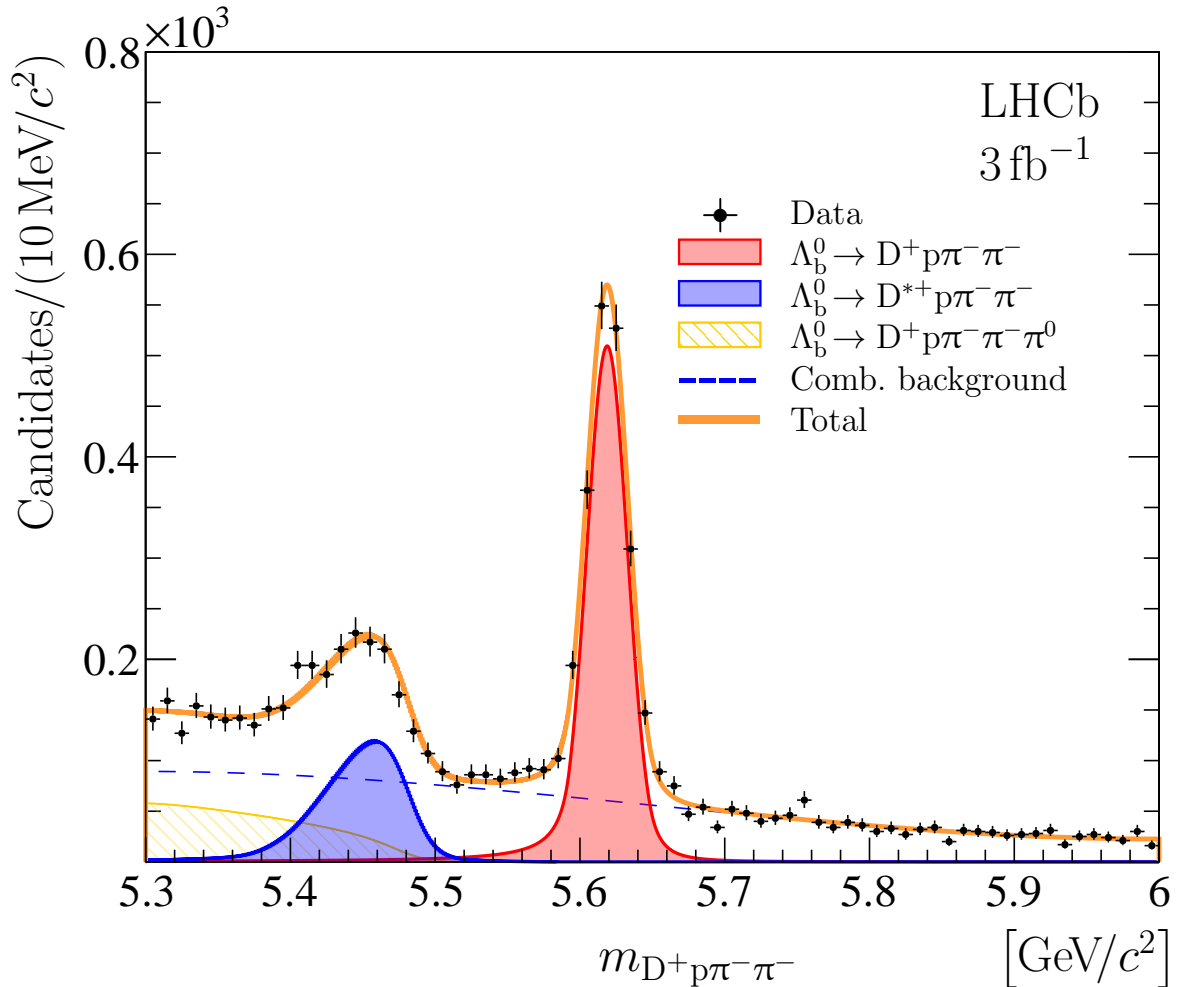


Figure 1: Mass distribution for selected $\Lambda_b^0 \rightarrow D^+ p \pi^- \pi^-$ candidates. The projection of an unbinned likelihood fit, described in the text, is superimposed.

power-law tails on both sides of the distribution [29, 30]. The tail parameters are fixed to values obtained from simulation, while the width and peak position are allowed to vary in the fit.

- A $\Lambda_b^0 \rightarrow D^{*+} p \pi^- \pi^-$ component, followed by $D^{*+} \rightarrow D^+ \pi^0$ and $D^{*+} \rightarrow D^+ \gamma$ decays. The shape of the component is taken from simulation and modified by a first order positive polynomial which accounts for the unknown Λ_b^0 decay model. The parameters of the polynomial function are allowed to vary in the fit.
- A $\Lambda_b^0 \rightarrow D^+ p \pi^- \pi^- \pi^0$ component, where the π^0 meson is undetected. The shape is also taken from simulation.
- A combinatorial-background component, parameterised with a positive monotonically-decreasing third-order polynomial function.

The fit result is overlaid on Fig. 1. The signal yields for the $\Lambda_b^0 \rightarrow D^+ p \pi^- \pi^-$ and $\Lambda_b^0 \rightarrow D^{*+} p \pi^- \pi^-$ decays are presented in Table 1. A similar four-component function is used to describe the $\Lambda_c^+ \pi^+ \pi^+ \pi^-$ mass spectrum.

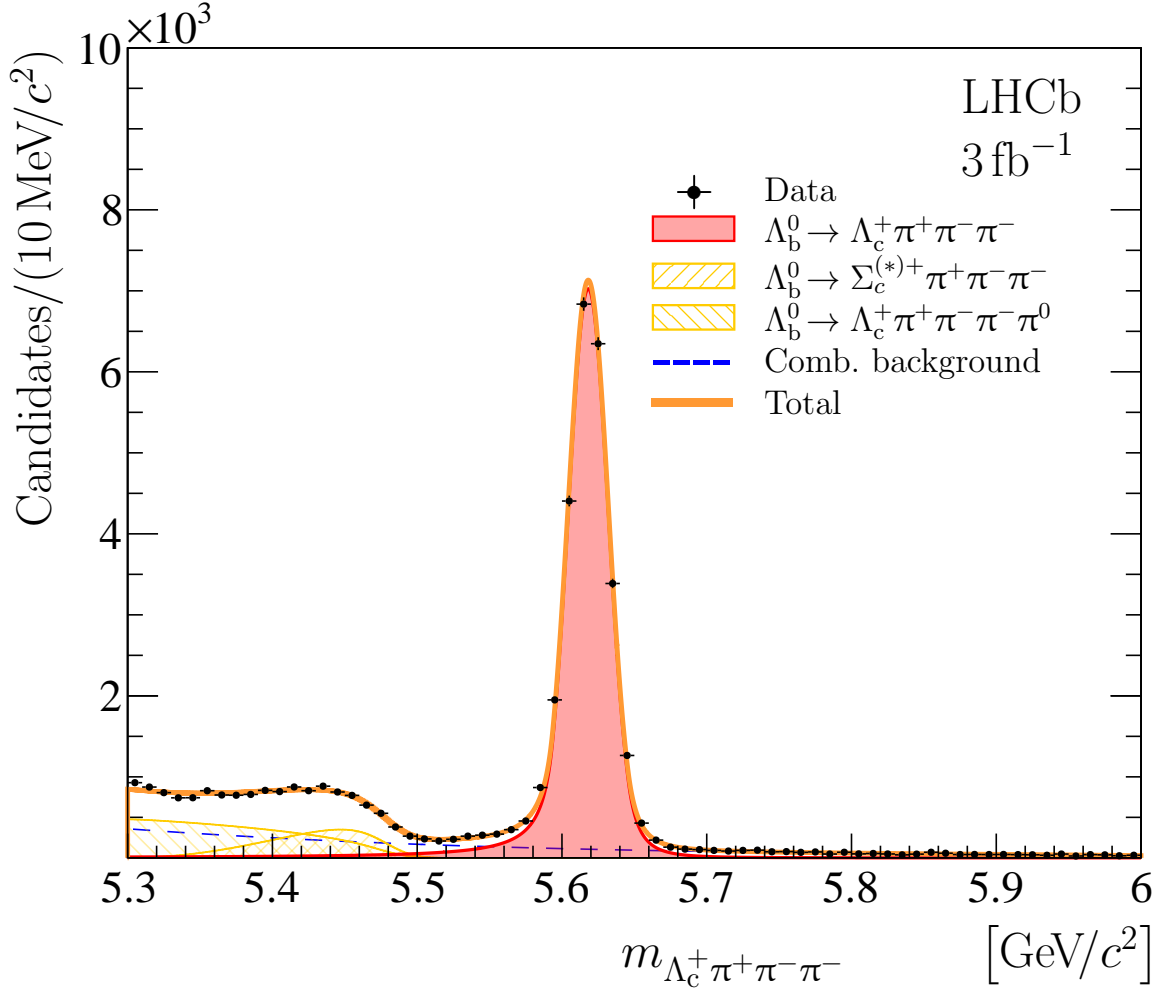


Figure 2: Mass distribution for selected $\Lambda_b^0 \rightarrow \Lambda_c^+ \pi^+ \pi^- \pi^-$ candidates. The projection of an unbinned likelihood fit, described in the text, is superimposed.

- A $\Lambda_b^0 \rightarrow \Lambda_c^+ \pi^+ \pi^- \pi^-$ component, parameterised with a modified Gaussian function with power-law tails on both sides of the distribution [29,30]. The tail parameters are fixed to values obtained from simulation, while the width and position are allowed to vary in the fit.
- A $\Lambda_b^0 \rightarrow \Sigma_c^{(*)+} \pi^+ \pi^- \pi^-$ component, followed by a $\Sigma_c^{(*)+} \rightarrow \Lambda_c^+ \pi^0$ decay with an undetected π^0 meson. The shape is taken from simulation.
- A $\Lambda_b^0 \rightarrow \Lambda_c^+ \pi^+ \pi^- \pi^- \pi^0$ component, where the π^0 meson is undetected. The shape is taken from simulation based on a phase-space decay model.
- A combinatorial-background component, parameterised with a positive monotonically-decreasing third-order polynomial function.

The fit result is overlaid on Fig. 2 and the signal yield for the $\Lambda_b^0 \rightarrow \Lambda_c^+ \pi^+ \pi^- \pi^-$ decays is presented in Table 1.

Several corrections, described below, are applied to the fitted yields. Since the $D^+ p \pi^- \pi^-$ channel with a $D^+ \rightarrow K^- \pi^+ \pi^+$ decay and the $\Lambda_c^+ \pi^+ \pi^- \pi^-$ channel

Table 1: Yields, N^{fit} , for the $\Lambda_b^0 \rightarrow D^+ p \pi^- \pi^-$, $\Lambda_b^0 \rightarrow D^{*+} p \pi^- \pi^-$ and $\Lambda_b^0 \rightarrow \Lambda_c^+ \pi^+ \pi^- \pi^-$ decays evaluated from fits to the $D^+ p \pi^- \pi^-$ and $\Lambda_c^+ \pi^+ \pi^- \pi^-$ mass spectra. The yields with all corrections described in the text, N^{cor} , are also given. The uncertainties are statistical only.

Decay mode	N^{fit}	N^{cor}
$\Lambda_b^0 \rightarrow D^+ p \pi^- \pi^-$	1933 ± 56	1542 ± 60
$\Lambda_b^0 \rightarrow D^{*+} p \pi^- \pi^-$	862 ± 55	875 ± 55
$\Lambda_b^0 \rightarrow \Lambda_c^+ \pi^+ \pi^- \pi^-$	$(26.51 \pm 0.18) \times 10^3$	$(25.91 \pm 0.18) \times 10^3$

with a $\Lambda_c^+ \rightarrow p K^- \pi^+$ decay consist of the same final state particles, there can be cross-feed between the two where true $\Lambda_b^0 \rightarrow \Lambda_c^+ \pi^+ \pi^- \pi^-$ decays are misreconstructed as $\Lambda_b^0 \rightarrow D^+ p \pi^- \pi^-$ decays. This contribution is studied using background-subtracted $p K^- \pi^+$ mass distributions from $\Lambda_b^0 \rightarrow D^+ p \pi^- \pi^-$ decays. The *sPlot* technique [31] is applied to the result of the fit described above, using the $D^+ p \pi^- \pi^-$ mass as the discriminating variable. The resulting background-subtracted $p K^- \pi_1^+ \pi_2^+$ mass spectra from the $\Lambda_b^0 \rightarrow D^+ p \pi^- \pi^-$ channel with $D^+ \rightarrow K^- \pi_1^+ \pi_2^+$ decays are shown in Fig. 3. The peaks at the known mass of the Λ_c^+ baryon correspond to true $\Lambda_b^0 \rightarrow \Lambda_c^+ \pi^+ \pi^- \pi^-$ decays reconstructed as $\Lambda_b^0 \rightarrow D^+ p \pi^- \pi^-$ decays. Fits are performed to these distributions with a function consisting of the following two terms.

- The $\Lambda_b^0 \rightarrow (\Lambda_c^+ \rightarrow p K^- \pi^+) \pi^+ \pi^- \pi^-$ contribution is modelled by a Gaussian function with the mean value and width taken from the fit to the $\Lambda_c^+ \rightarrow p K^- \pi^+$ signal from $\Lambda_b^0 \rightarrow (\Lambda_c^+ \rightarrow p K^- \pi^+) \pi^+ \pi^- \pi^-$ decays.
- A first-order polynomial term models the baseline background from Λ_b^0 baryon decays without a Λ_c^+ baryon in the final state.

This fit yields 395 ± 23 misreconstructed $\Lambda_b^0 \rightarrow (D^+ \rightarrow K^- \pi^+ \pi^+) p \pi^- \pi^-$ candidates, which are subtracted from the total fit yield of the $\Lambda_b^0 \rightarrow D^+ p \pi^- \pi^-$ mode. No analogous pattern is observed in the background-subtracted $p K^- \pi^+$ mass spectra from $\Lambda_b^0 \rightarrow D^{*+} p \pi^- \pi^-$ decays. Possible cross-feed from $\Lambda_b^0 \rightarrow D^{(*)+} p \pi^- \pi^-$ decays in the $\Lambda_b^0 \rightarrow (\Lambda_c^+ \rightarrow p K^- \pi^+) \pi^+ \pi^- \pi^-$ normalisation signal is found to be negligible.

The background-subtracted $\pi^+ \pi^- \pi^-$ mass spectrum from $\Lambda_b^0 \rightarrow \Lambda_c^+ \pi^+ \pi^- \pi^-$ decays is shown in Fig. 4 (left), where background subtraction is performed with the *sPlot* technique using the $\Lambda_c^+ \pi^+ \pi^- \pi^-$ mass as the discriminating variable. A small contribution from $\Lambda_b^0 \rightarrow \Lambda_c^+ D_s^-$ decays, followed by the $D_s^- \rightarrow \pi^+ \pi^- \pi^-$ decay, is visible in the $\pi^+ \pi^- \pi^-$ mass spectrum [32]. A fit to the background-subtracted $\pi^+ \pi^- \pi^-$ mass distribution is performed with a Gaussian function summed with a positive first-order polynomial function. The Gaussian mean is set to the known mass of the D_s^- meson [27], while the resolution is taken from the fit to a larger data sample available at an earlier stage of the selection. The polynomial function models the $\Lambda_b^0 \rightarrow \Lambda_c^+ \pi^+ \pi^- \pi^-$ decays without an intermediate D_s^- meson. The fit yields 176 ± 25 $\Lambda_b^0 \rightarrow \Lambda_c^+ D_s^-$ decays, which are subtracted from the total fitted yield of the $\Lambda_b^0 \rightarrow \Lambda_c^+ \pi^+ \pi^- \pi^-$ decays.

A small fraction of $\Lambda_b^0 \rightarrow (\Lambda_c^+ \rightarrow p K^- \pi_1^+) \pi_2^+ \pi^- \pi^-$ decays satisfies all selection criteria after the interchange of two positive pions, $\pi_1^+ \leftrightarrow \pi_2^+$, causing the same six-track combination to be reconstructed twice. This effect is studied using the background-subtracted

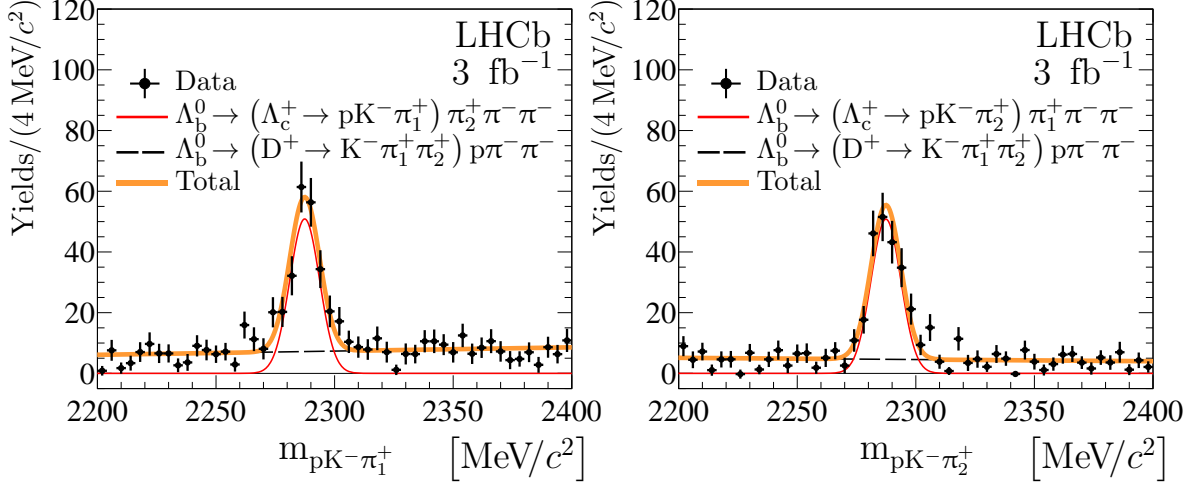


Figure 3: Background-subtracted $pK^- \pi_{1,2}^+$ mass spectra from the $\Lambda_b^0 \rightarrow D^+ p \pi^- \pi^-$ channel with $D^+ \rightarrow K^- \pi_1^+ \pi_2^+$ decays.

$pK^- \pi_2^+$ mass distribution from the selected $\Lambda_b^0 \rightarrow (\Lambda_c^+ \rightarrow pK^- \pi_1^+) \pi_2^+ \pi^- \pi^-$ decays, shown in Fig. 4 (right). Duplicate candidates appear near the known mass of the Λ_c^+ baryon. A fit to the $pK^- \pi_2^+$ mass distribution is performed using a Gaussian function for the $\Lambda_b^0 \rightarrow (\Lambda_c^+ \rightarrow pK^- \pi_2^+) \pi_1^+ \pi^- \pi^-$ decays and a first-order polynomial function for the $\Lambda_b^0 \rightarrow (\Lambda_c^+ \rightarrow pK^- \pi_1^+) \pi_2^+ \pi^- \pi^-$ decays. The mean and width of the Gaussian function are taken from a fit to the $\Lambda_c^+ \rightarrow pK^- \pi^+$ candidates from $\Lambda_b^0 \rightarrow (\Lambda_c^+ \rightarrow pK^- \pi^+) \pi^+ \pi^- \pi^-$ decays. The $\Lambda_b^0 \rightarrow (\Lambda_c^+ \rightarrow pK^- \pi_2^+) \pi_1^+ \pi^- \pi^-$ yield is 416 ± 32 , and is subtracted from the total fit yield of the $\Lambda_b^0 \rightarrow \Lambda_c^+ \pi^+ \pi^- \pi^-$ decays.

Possible biases in the yields of the $\Lambda_b^0 \rightarrow D^{(*)+} p \pi^- \pi^-$ and $\Lambda_b^0 \rightarrow \Lambda_c^+ \pi^+ \pi^- \pi^-$ decays from the relevant fits are studied using pseudoexperiments. The largest bias is found for the yield of $\Lambda_b^0 \rightarrow D^{*+} p \pi^- \pi^-$ decays and it is 1.5%. For the $\Lambda_b^0 \rightarrow D^+ p \pi^- \pi^-$ and $\Lambda_b^0 \rightarrow \Lambda_c^+ \pi^+ \pi^- \pi^-$ decays the corresponding biases are much smaller. The final yields, after all corrections described above are applied, are given in Table 1 for the $\Lambda_b^0 \rightarrow D^{(*)+} p \pi^- \pi^-$ and $\Lambda_b^0 \rightarrow \Lambda_c^+ \pi^+ \pi^- \pi^-$ decays.

5 Efficiency and ratios of branching fractions

The ratios \mathcal{R}_{D^+} and $\mathcal{R}_{D^{*+}}$, defined by Eq. (1) are calculated as

$$\mathcal{R}_{D^+} = \frac{N_{\Lambda_b^0 \rightarrow D^+ p \pi^- \pi^-}^{\text{cor}}}{N_{\Lambda_b^0 \rightarrow \Lambda_c^+ \pi^+ \pi^- \pi^-}^{\text{cor}}} \times \frac{\varepsilon_{\Lambda_b^0 \rightarrow \Lambda_c^+ \pi^+ \pi^- \pi^-}}{\varepsilon_{\Lambda_b^0 \rightarrow D^+ p \pi^- \pi^-}} \quad (2a)$$

and

$$\mathcal{R}_{D^{*+}} = \frac{N_{\Lambda_b^0 \rightarrow D^{*+} p \pi^- \pi^-}^{\text{cor}}}{N_{\Lambda_b^0 \rightarrow D^+ p \pi^- \pi^-}^{\text{cor}}} \times \frac{\varepsilon_{\Lambda_b^0 \rightarrow D^+ p \pi^- \pi^-}}{\varepsilon_{\Lambda_b^0 \rightarrow D^{*+} p \pi^- \pi^-}}, \quad (2b)$$

where N_X^{cor} is the corrected signal yield for decay mode X , as per Table 1, and ε_X is the corresponding efficiency. This efficiency is defined as a product of the detector

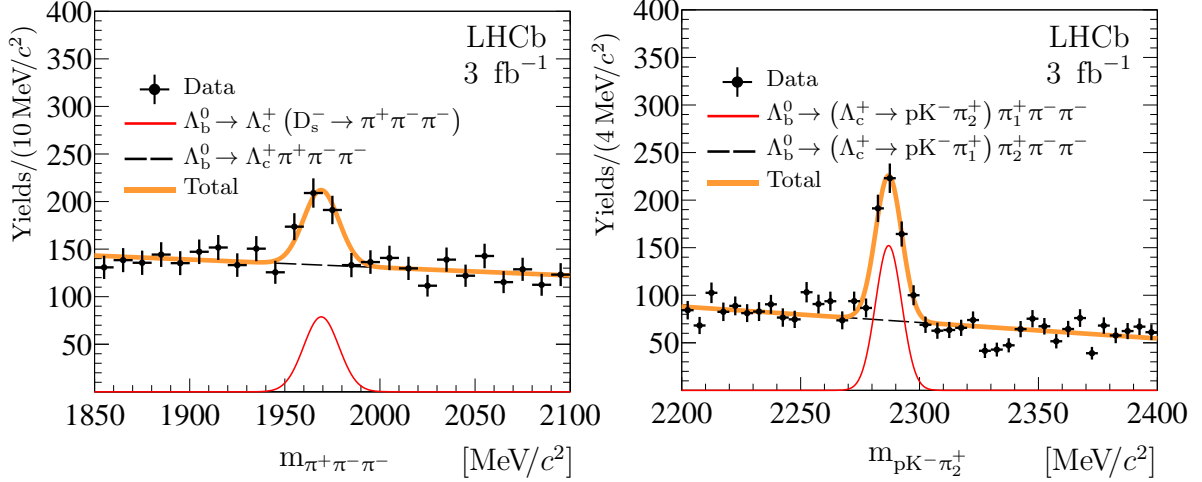


Figure 4: Background-subtracted (left) $\pi^+\pi^-\pi^-$ mass distribution from $\Lambda_b^0 \rightarrow \Lambda_c^+\pi^+\pi^-\pi^-$ decays and (right) $pK^-\pi_2^+$ mass distribution from $\Lambda_b^0 \rightarrow (\Lambda_c^+ \rightarrow pK^-\pi_1^+)\pi_2^+\pi^-\pi^-$ decays. The results of the fits described in text are overlaid.

acceptance ε^{acc} , reconstruction and selection efficiency $\varepsilon^{\text{rec\&sel}}$, efficiency of the hardware stage of the trigger ε^{trg} and the hadron-identification efficiency ε^{PID} ,

$$\varepsilon = \varepsilon^{\text{acc}} \varepsilon^{\text{rec\&sel}} \varepsilon^{\text{trg}} \varepsilon^{\text{PID}}, \quad (3)$$

where each subsequent efficiency is defined with respect to the product of previous efficiencies. The detector acceptance, and reconstruction and selection efficiency, are determined using the simulation samples described in Sec. 2. The reconstruction and selection efficiency is corrected for a small difference in the track reconstruction efficiency between data and simulation [24]. The trigger efficiency is calculated from single-particle hadron-trigger efficiencies, which are determined separately for protons, kaons and pions from a large $\Lambda_b^0 \rightarrow (\Lambda_c^+ \rightarrow pK^-\pi^+)\pi^-$ data sample. The hadron-identification efficiency is a combination of single-particle identification efficiencies for protons, kaons and pions determined with large calibration samples of $\Lambda_c^+ \rightarrow pK^-\pi^+$, $\Lambda \rightarrow p\pi^-$, $D^{*+} \rightarrow (D^0 \rightarrow K^-\pi^+)\pi^+$, $D_s^+ \rightarrow (\phi \rightarrow K^+K^-)\pi^+$ and $K_S^0 \rightarrow \pi^+\pi^-$ decays in data [26]. The ratios of efficiencies are,

$$\frac{\varepsilon_{\Lambda_b^0 \rightarrow D^+ p \pi^- \pi^-}}{\varepsilon_{\Lambda_b^0 \rightarrow \Lambda_c^+ \pi^+ \pi^- \pi^-}} = 1.11 \pm 0.01 \quad (4a)$$

and

$$\frac{\varepsilon_{\Lambda_b^0 \rightarrow D^{*+} p \pi^- \pi^-}}{\varepsilon_{\Lambda_b^0 \rightarrow D^+ p \pi^- \pi^-}} = 0.93 \pm 0.01, \quad (4b)$$

where the uncertainties arise from the finite size of the simulation samples. Using the corrected yields from Table 1 and efficiencies from Eq. (4), the ratios \mathcal{R}_{D^+} and $\mathcal{R}_{D^{*+}}$ are found to be

$$\mathcal{R}_{D^+} = (5.35 \pm 0.21) \% \quad (5a)$$

and

$$\mathcal{R}_{D^{*+}} = (61.3 \pm 4.3) \%, \quad (5b)$$

where the uncertainties are statistical only. Systematic uncertainties are discussed in Sec. 6.

The background-subtracted two- and three-body mass spectra from the $\Lambda_b^0 \rightarrow D^+ p \pi^- \pi^-$ and $\Lambda_b^0 \rightarrow D^{*+} p \pi^- \pi^-$ decays are shown in Figs. 5 through 8 with the expectation from phase-space simulated decays overlaid. The analogous distributions for the $\Lambda_b^0 \rightarrow \Lambda_c^+ \pi^+ \pi^- \pi^-$ decays are shown in Appendix A; corresponding distributions from the corrected simulation samples, used for evaluation of the efficiencies, are also shown. Large deviations between data and phase-space based simulation are observed, demonstrating a rich structure of intermediate resonances for the decay of this study.

6 Systematic uncertainties

Due to the shared analysis techniques used to determine the yields for the $\Lambda_b^0 \rightarrow D^{(*)+} p \pi^- \pi^-$ and $\Lambda_b^0 \rightarrow \Lambda_c^+ \pi^+ \pi^- \pi^-$ decays, many systematic uncertainties cancel for the ratios \mathcal{R}_{D^+} and $\mathcal{R}_{D^{*+}}$. The remaining contributions to systematic uncertainty are summarised in Table 2 and discussed below.

An important source of systematic uncertainty on the ratios of the branching fractions arises from the imperfect knowledge of the mass shapes of the signal and background components used in the fits. To estimate this uncertainty, several alternative models for the signal and background components are tested. For the $\Lambda_b^0 \rightarrow D^+ p \pi^- \pi^-$ and $\Lambda_b^0 \rightarrow \Lambda_c^+ \pi^+ \pi^- \pi^-$ signal shapes the tail parameters of modified Gaussian functions are varied within uncertainties, determined from fits to corresponding simulation samples. The order of the positive monotonically-decreasing polynomial function,

Table 2: Relative systematic uncertainties for the ratios \mathcal{R}_{D^+} and $\mathcal{R}_{D^{*+}}$. The total uncertainty is obtained by summing all terms in quadrature.

Source	$\sigma_{\mathcal{R}_{D^+}}$ [%]	$\sigma_{\mathcal{R}_{D^{*+}}}$ [%]
Fit model	1.5	5.7
Multiple candidates	0.8	0.7
Λ_b^0 kinematic spectra	0.2	0.4
$\Lambda_b^0 \rightarrow D^{(*)+} p \pi^- \pi^-$ decay model	0.1	0.2
$\Lambda_b^0 \rightarrow \Lambda_c^+ \pi^+ \pi^- \pi^-$ decay model	0.3	—
Hadron identification	0.7	0.5
Tracking efficiency	0.2	0.0
Hardware-trigger efficiency	0.9	0.5
Data-simulation difference	1.9	2.8
Simulation samples size	0.8	0.9
Total	2.9	6.5

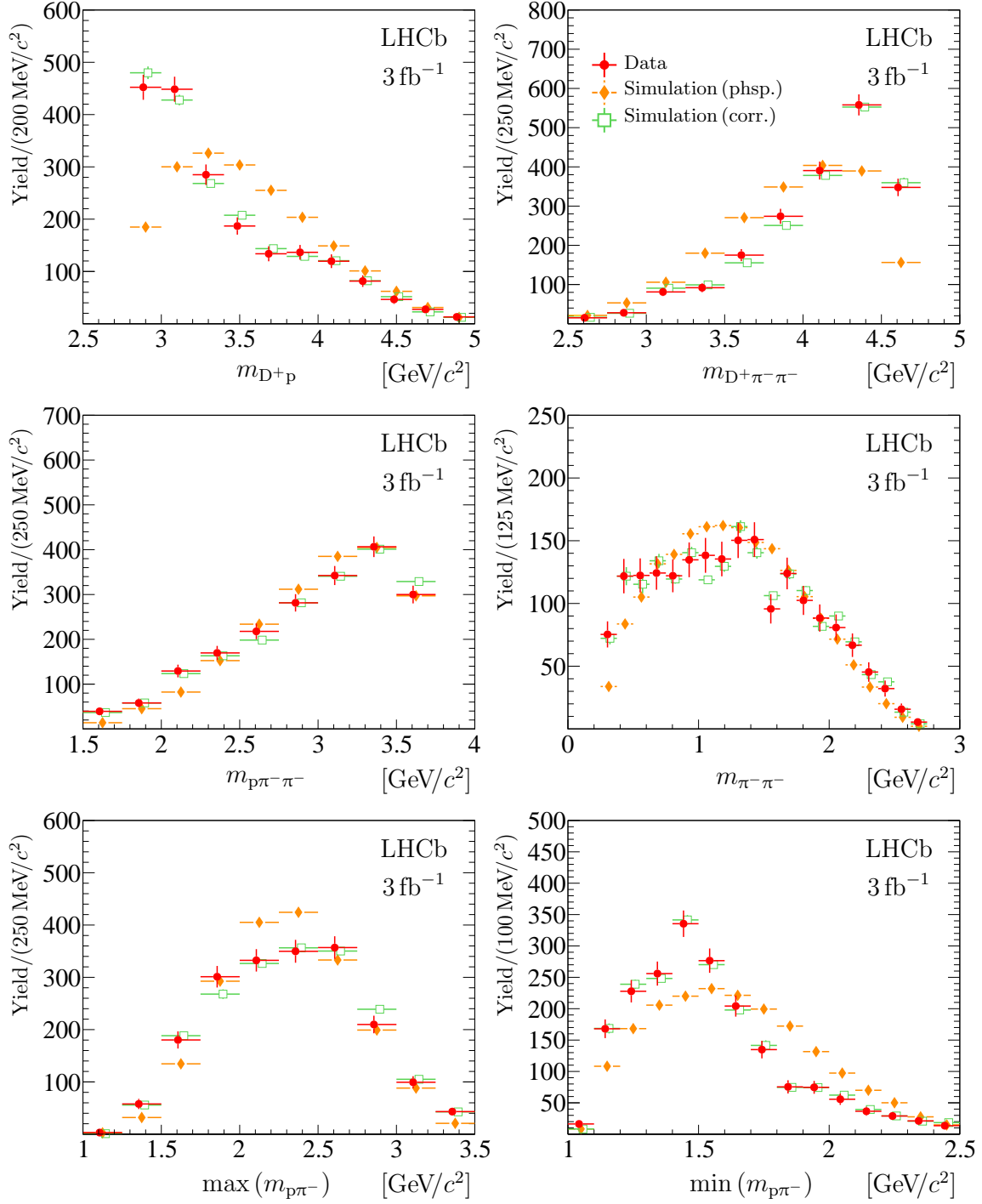


Figure 5: Background-subtracted D^+p , $D^+\pi^-\pi^-$, $p\pi^-\pi^-$, $\pi^-\pi^-$, and maximum and minimum $p\pi^-$ mass spectra for $\Lambda_b^0 \rightarrow D^+p\pi^-\pi^-$ decays. Expectations from phase-space (phsp.) and corrected (corr.) simulation are overlaid.

used for modelling of the background components, is varied between two and four. The ratio of branching fractions for the $D^{*+} \rightarrow D^+\gamma$ and $D^{*+} \rightarrow D^+\pi^0$ decays affects the shape of the $\Lambda_b^0 \rightarrow D^{*+}p\pi^-\pi^-$ component. This ratio is varied within the known uncertainty [27, 33, 34]. For the $\Lambda_b^0 \rightarrow D^{*+}p\pi^-\pi^-$ fit component, the polynomial factor

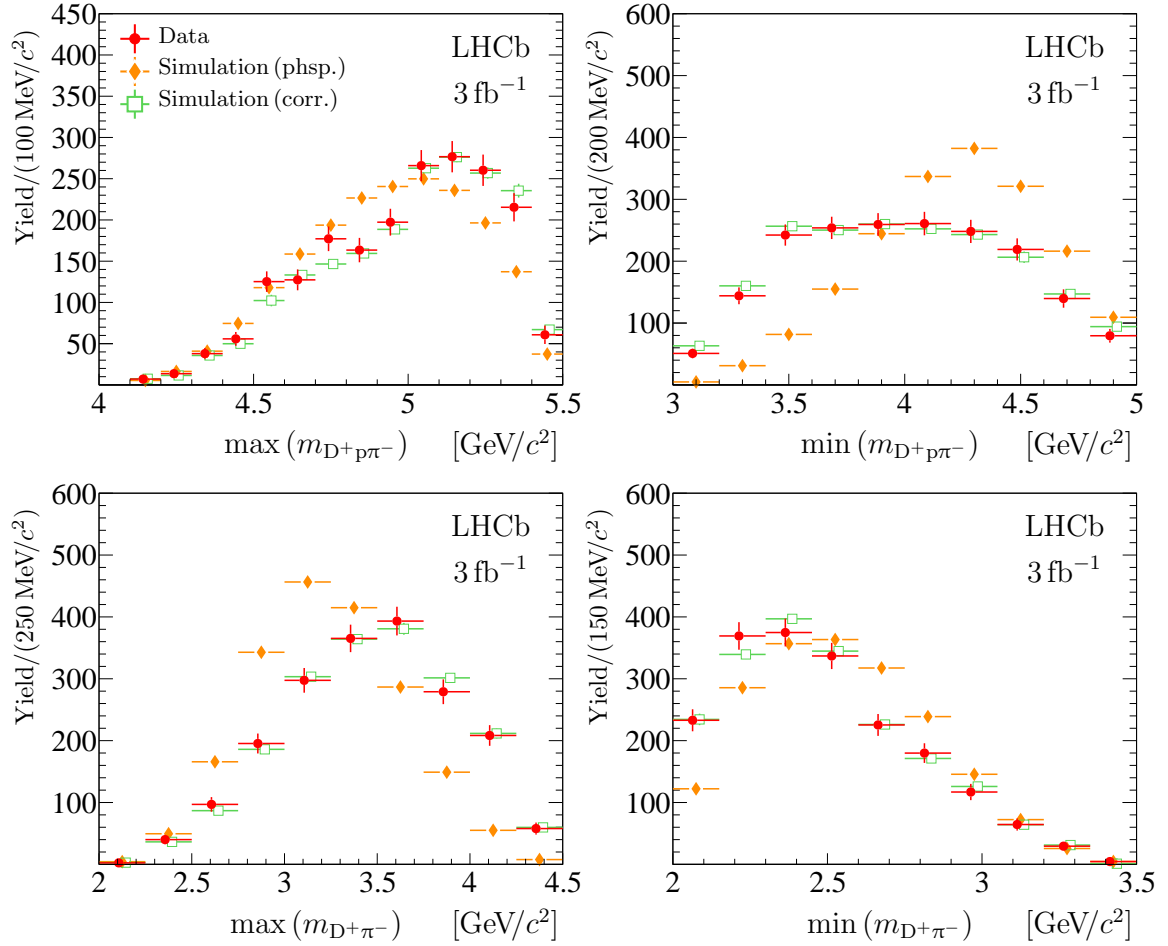


Figure 6: Background-subtracted maximum and minimum $D^+ p \pi^-$, and maximum and minimum $D^+ \pi^-$ mass spectra for $\Lambda_b^0 \rightarrow D^+ p \pi^- \pi^-$ decays. Expectations from phase-space (phsp.) and corrected (corr.) simulation are overlaid.

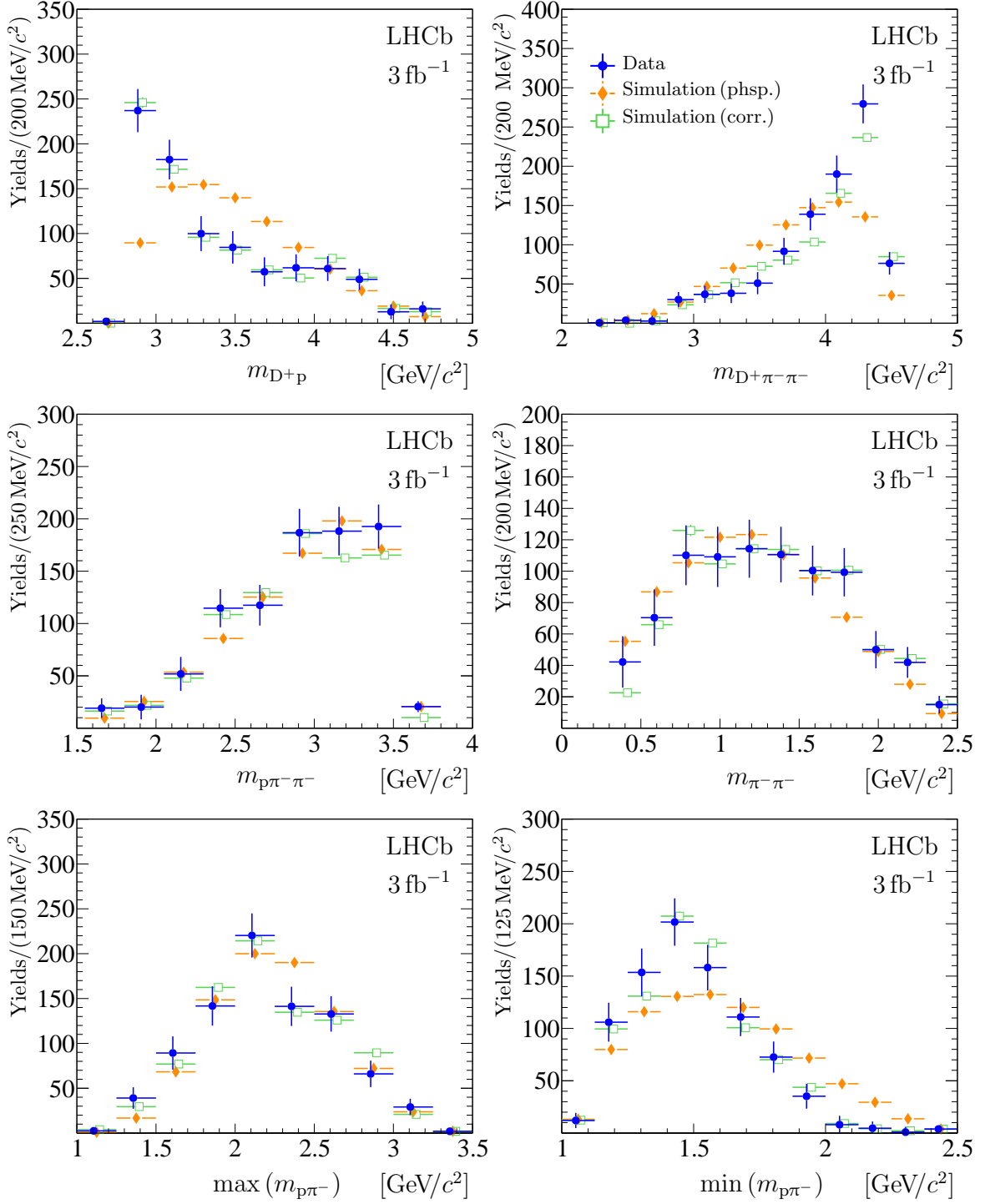


Figure 7: Background-subtracted D^+p , $D^+\pi^-\pi^-$, $p\pi^-\pi^-$, $\pi^-\pi^-$, and maximum and minimum $p\pi^-$ mass spectra for $\Lambda_b^0 \rightarrow D^+p\pi^-\pi^-$ decays. Expectations from phase-space (phsp.) and corrected (corr.) simulation are overlaid.

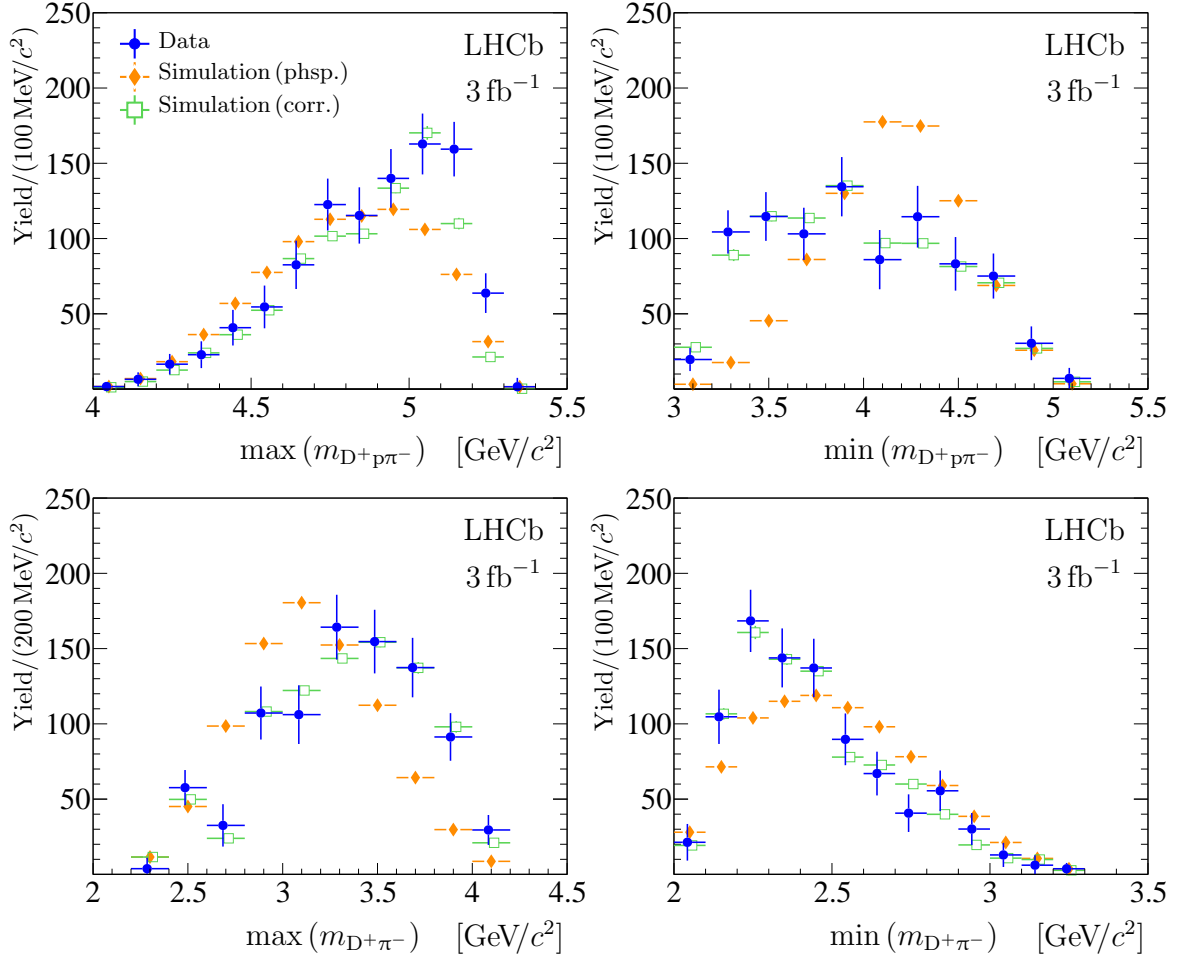


Figure 8: Background-subtracted maximum and minimum $D^+ p \pi^-$, and maximum and minimum $D^+ \pi^-$ mass spectra for $\Lambda_b^0 \rightarrow D^{*+} p \pi^- \pi^-$ decays. Expectations from phase-space (phsp.) and corrected (corr.) simulation are overlaid.

that modifies the shape obtained from the simulation is removed. For each alternative model the ratio of event yields is determined, and the maximal deviation with respect to the default model is taken as the systematic uncertainty. This uncertainty is 1.5% and 5.7% for the ratios \mathcal{R}_{D^+} and $\mathcal{R}_{D^{*+}}$, respectively.

A small fraction of events contain multiple Λ_b^0 candidates. These Λ_b^0 candidates have an approximately uniform mass distribution between 5.3 and 6.0 GeV/ c^2 . To estimate the uncertainty associated with the presence of multiple Λ_b^0 candidates, a single random Λ_b^0 candidate is kept, while the other candidates are discarded and the ratios of the event yields are measured. This procedure is repeated for multiple trials to mitigate the effects of statistical fluctuations. The differences between the original mean values of \mathcal{R}_{D^+} and $\mathcal{R}_{D^{*+}}$ and the values obtained using randomisation are found to be 0.8% and 0.7%, respectively. These differences are taken as systematic uncertainty associated with the selection of multiple candidates.

The transverse momentum and rapidity spectra of Λ_b^0 baryons in the simulation samples are corrected to reproduce those observed for the $\Lambda_b^0 \rightarrow \Lambda_c^+ \pi^+ \pi^- \pi^-$ signal in data. This correction is a source of additional uncertainty, which is evaluated with several sets of corrections obtained using different interval schemes for the p_T and rapidity distributions of the Λ_b^0 candidates. These corrections are applied to the simulation samples and maximal deviations of 0.2% and 0.4% are observed for the ratios \mathcal{R}_{D^+} and $\mathcal{R}_{D^{*+}}$, respectively. These deviations are set as the systematic uncertainty due to imperfect knowledge of the production spectra of the Λ_b^0 baryons.

The simulated $\Lambda_b^0 \rightarrow D^+ p \pi^- \pi^-$, $\Lambda_b^0 \rightarrow D^{*+} p \pi^- \pi^-$ and $\Lambda_b^0 \rightarrow \Lambda_c^+ \pi^+ \pi^- \pi^-$ samples are corrected to reproduce the two- and three-body signal mass distributions observed in data. Due to a large number of variables and their correlations, the method requires several iterations to converge. The corrections made for binned distributions are illustrated in Figs. 5 through 8 for the $\Lambda_b^0 \rightarrow D^+ p \pi^- \pi^-$, $\Lambda_b^0 \rightarrow D^{*+} p \pi^- \pi^-$ samples and Figs. A1 and A2 for the $\Lambda_b^0 \rightarrow \Lambda_c^+ \pi^+ \pi^- \pi^-$ sample. To estimate the systematic uncertainty related to the imperfect knowledge of the decay model for $\Lambda_b^0 \rightarrow D^{(*)+} p \pi^- \pi^-$ and $\Lambda_b^0 \rightarrow \Lambda_c^+ \pi^+ \pi^- \pi^-$ decays, the number of iterations is varied. The differences with respect to the baseline results for the \mathcal{R}_{D^+} and $\mathcal{R}_{D^{*+}}$ ratios are assigned as systematic uncertainty due to the imperfect knowledge of the $\Lambda_b^0 \rightarrow D^{(*)+} p \pi^- \pi^-$ and $\Lambda_b^0 \rightarrow \Lambda_c^+ \pi^+ \pi^- \pi^-$ decay models.

The hadron-identification efficiency for protons, kaons and pions is estimated using large calibration samples. The uncertainty due to the finite size of the calibration samples is propagated to the ratios \mathcal{R}_{D^+} and $\mathcal{R}_{D^{*+}}$ using pseudoexperiments. The obtained variations of 0.7% and 0.5% for the \mathcal{R}_{D^+} and $\mathcal{R}_{D^{*+}}$ ratios, respectively, are used as the systematic uncertainty associated to the hadron identification.

There are residual differences in the reconstruction efficiency of charged-particle tracks that do not cancel completely in the ratio due to small differences in the kinematic distributions of the final-state particles. The track-finding efficiencies obtained from simulation samples are corrected using calibration modes [24]. The uncertainties related to the efficiency correction factors are propagated to the ratios of the total efficiencies using pseudoexperiments and are determined as 0.2% and smaller than 0.1% for the \mathcal{R}_{D^+} and $\mathcal{R}_{D^{*+}}$ ratios, respectively. These values are taken as the systematic uncertainty associated with the tracking efficiency.

The hardware-trigger efficiency for protons, kaons and pions is estimated using a large $\Lambda_b^0 \rightarrow (\Lambda_c^+ \rightarrow p K^- \pi^+) \pi^-$ calibration sample. Efficiencies from alternative calibration samples, *e.g.* $D^{*+} \rightarrow (D^0 \rightarrow K^- \pi^+) \pi^+$ decays, yield 0.9% and 0.5% variations for the \mathcal{R}_{D^+}

and $\mathcal{R}_{D^{*+}}$ ratios, respectively. These variations are taken as the systematic uncertainty due to the hardware-trigger efficiency.

The stability of the results is checked by changing the selection criteria on transverse momenta for the final state hadrons, the χ^2 from the kinematic fit and decay time for Λ_b^0 candidates. The ratios \mathcal{R}_{D^+} and $\mathcal{R}_{D^{*+}}$ vary by up to 1.9% and 2.8%, respectively, and these variations are conservatively assigned as a systematic uncertainty due to data-simulation differences not considered elsewhere. Finally, the 0.8% and 0.9% relative uncertainties from Eq. (4) are assigned as a systematic uncertainty due to the finite size of the simulated samples for the \mathcal{R}_{D^+} and $\mathcal{R}_{D^{*+}}$ ratios, respectively.

7 Results and summary

The decays $\Lambda_b^0 \rightarrow D^+ p \pi^- \pi^-$ and $\Lambda_b^0 \rightarrow D^{*+} p \pi^- \pi^-$ are observed using data collected with the LHCb detector in proton-proton collisions corresponding to 1 and 2 fb^{-1} of integrated luminosity at centre-of-mass energies of 7 and 8 TeV, respectively. Both decay modes belong to the relatively unexplored class of beauty-baryon decays where the c -quark from the $b \rightarrow c$ transition hadronises into the final state separate from the baryon, *i.e.* a charm meson and a proton. These multihadron decays exhibit a rich resonance structure.

Using the $\Lambda_b^0 \rightarrow \Lambda_c^+ \pi^+ \pi^- \pi^-$ decay as a normalisation channel, the ratios of branching fractions defined by Eq. (1) are measured to be

$$\mathcal{R}_{D^+} = (5.35 \pm 0.21 \pm 0.16) \%$$

and

$$\mathcal{R}_{D^{*+}} = (61.3 \pm 4.3 \pm 4.0) \%,$$

where the first uncertainty is statistical and the second systematic.

The relative rate for $\Lambda_b^0 \rightarrow D^{*+} p \pi^+ \pi^+$ and $\Lambda_b^0 \rightarrow D^+ p \pi^+ \pi^+$ decays r_{D^*} is defined as

$$r_{D^{*+}} \equiv \frac{\mathcal{B}(\Lambda_b^0 \rightarrow D^{*+} p \pi^+ \pi^+)}{\mathcal{B}(\Lambda_b^0 \rightarrow D^+ p \pi^+ \pi^+)} = \frac{\mathcal{R}_{D^{*+}}}{\mathcal{B}(D^{*+} \rightarrow D^+ \pi^0 / \gamma)}.$$

Using the known branching fractions of the D^{*+} meson [27], the ratio $r_{D^{*+}}$ is 1.9 ± 0.2 . For multihadron $b \rightarrow c$ decays with a large energy release, a relative yield of the D^{*+} and D^+ mesons is expected to be similar to one for the D^{*+} and D^+ mesons produced via a charm quark fragmentation in high-energy hadron or e^+e^- interactions. A naïve spin-counting rule [35, 36] predicts the ratio $r_{D^{*+}}$ to be as large as 3. The relative production of D^{*+} and D^+ mesons produced promptly in pp collisions at $\sqrt{s} = 5, 7$ and 13 TeV is estimated using the cross sections of directly produced D^{*+} and D^+ mesons, $\sigma_{pp \rightarrow D^{*+} X}^{\text{direct}}$ and $\sigma_{pp \rightarrow D^+ X}^{\text{direct}}$, as

$$r_{D^{*+}}^{\text{pp}} \equiv \frac{\sigma_{pp \rightarrow D^{*+} X}^{\text{direct}}}{\sigma_{pp \rightarrow D^+ X}^{\text{direct}}} \approx \frac{\sigma_{pp \rightarrow D^{*+} X}}{\sigma_{pp \rightarrow D^+ X} - \mathcal{B}(D^{*+} \rightarrow D^+ \pi^0 / \gamma) \times \sigma_{pp \rightarrow D^{*+} X}},$$

where $\sigma_{pp \rightarrow D^{*+} X}$ and $\sigma_{pp \rightarrow D^+ X}$ are the measured inclusive cross sections of the promptly produced D^{*+} and D^+ mesons. Assuming an independent fragmentation of the c quark

into D^{*+} and D^+ mesons in direct production, and averaging $r_{D^{*+}}^{\text{pp}}$ over the different proton collision energies of 5, 7, and 13 TeV [37–39], the value $r_{D^{*+}}^{\text{pp}}$ is 1.5 ± 0.1 . The obtained value is smaller than the value of $r_{D^{*+}}$ obtained from the $\Lambda_b^0 \rightarrow D^{(*)+} p \pi^- \pi^-$ decays, but consistent within two standard deviations. The value for the ratio of production cross-sections of D^{*+} and D^+ mesons in e^+e^- collisions, $r_{D^{*+}}^{e^+e^-} = 1.86 \pm 0.16$, from Ref. [36] is obtained from a combination of measurements performed by the CLEO [40], ARGUS [41], ALEPH [42] and VENUS [43] collaborations analysing data from high energy e^+e^- annihilation. The similarity between these values indicates a possible correspondence between direct charm-meson production and fragmentation, and charm-meson production in the multihadron decays of beauty hadrons.

Analysis of the $\Lambda_c^+ \pi^+ \pi^- \pi^-$ spectra shows that $\Lambda_b^0 \rightarrow \Sigma_c^{(*)+} \pi^+ \pi^- \pi^-$ decays are largely suppressed with respect to $\Lambda_b^0 \rightarrow \Lambda_c^+ \pi^+ \pi^- \pi^-$ decays, see Fig. 2. The relative production of charmed $\Sigma_c^{(*)+}$ and Λ_c^+ baryons exhibits the same trend both in e^+e^- annihilation [44] and in high energy hadroproduction [45]. From these measurements, a consistent picture emerges where formation and production of a light isoscalar diquark that is a scalar is more favourable during the hadronisation of heavy charm quarks, than a light isovector diquark that is an axial vector [46–48]. This observation supports the diquark model for heavy-flavor baryon structure and production [49].

In conclusion, $\Lambda_b^0 \rightarrow D^+ p \pi^- \pi^-$ and $\Lambda_b^0 \rightarrow D^{*+} p \pi^- \pi^-$ decays are observed for the first time and their relative branching ratios are measured. Both these decays, and the $\Lambda_b^0 \rightarrow \Lambda_c^+ \pi^+ \pi^- \pi^-$ decays used in this analysis as a normalisation channel, demonstrate a rich resonance structure. A similarity between prompt charm-meson production and charm-meson production from multihadron decays of Λ_b^0 baryons is observed. In the future, the observed decay $\Lambda_b^0 \rightarrow D^+ p \pi^- \pi^-$ can serve as a normalisation mode for studies of similar rare decays, *e.g.* $\Xi_b^0 \rightarrow D^+ p K^- \pi^-$ and $\Xi_b^0 \rightarrow D^{*+} p K^- \pi^-$ decays.

Acknowledgements

We express our gratitude to our colleagues in the CERN accelerator departments for the excellent performance of the LHC. We thank the technical and administrative staff at the LHCb institutes. We acknowledge support from CERN and from the national agencies: CAPES, CNPq, FAPERJ and FINEP, (Brazil); MOST and NSFC (China); CNRS/IN2P3 (France); BMBF, DFG and MPG (Germany); INFN (Italy); NWO (Netherlands); MNiSW and NCN (Poland); MEN/IFA (Romania); MSHE (Russia); MICINN (Spain); SNSF and SER (Switzerland); NASU (Ukraine); STFC (United Kingdom); DOE NP and NSF (USA). We acknowledge the computing resources that are provided by CERN, IN2P3 (France), KIT and DESY (Germany), INFN (Italy), SURF (Netherlands), PIC (Spain), GridPP (United Kingdom), RRCKI and Yandex LLC (Russia), CSCS (Switzerland), IFIN-HH (Romania), CBPF (Brazil), PL-GRID (Poland) and NERSC (USA). We are indebted to the communities behind the multiple open-source software packages on which we depend. Individual groups or members have received support from ARC and ARDC (Australia); AvH Foundation (Germany); EPLANET, Marie Skłodowska-Curie Actions and ERC (European Union); A*MIDEX, ANR, IPhU and Labex P2IO, and Région Auvergne-Rhône-Alpes (France); Key Research Program of Frontier Sciences of CAS, CAS PIFI, CAS CCEPP, Fundamental Research Funds for the Central Universities, and Sci. & Tech. Program of Guangzhou (China);

RFBR, RSF and Yandex LLC (Russia); GVA, XuntaGal and GENCAT (Spain); the Leverhulme Trust, the Royal Society and UKRI (United Kingdom).

A Mass spectra for $\Lambda_b^0 \rightarrow \Lambda_c^+ \pi^+ \pi^- \pi^-$ decays

Background-subtracted two- and three-body mass spectra for the $\Lambda_b^0 \rightarrow \Lambda_c^+ \pi^+ \pi^- \pi^-$ decays are shown in Figs. A1 and A2. A rich structure of intermediate resonances is visible.

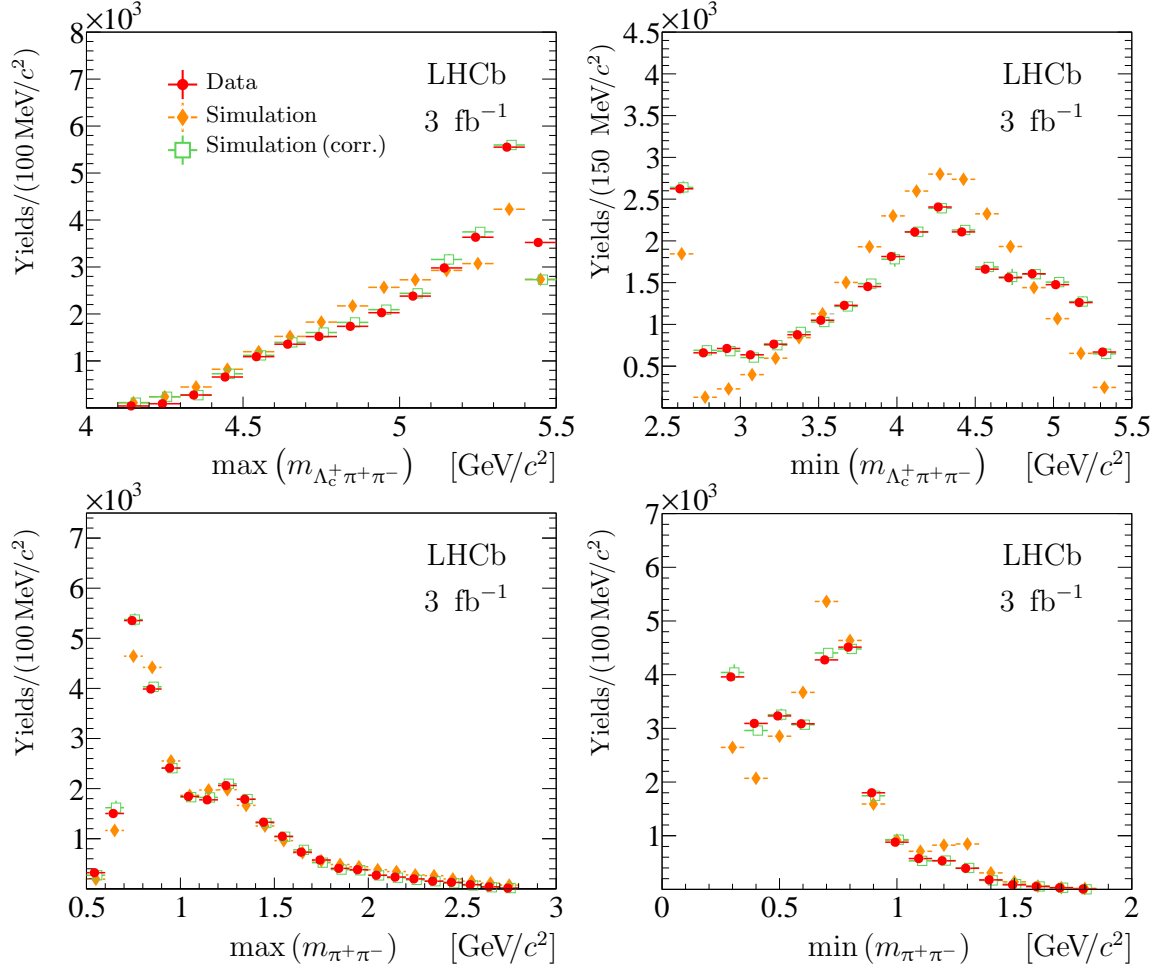


Figure A1: Background-subtracted maximum and minimum $\Lambda_c^+ \pi^+ \pi^-$, and maximum and minimum $\pi^+ \pi^-$ mass spectra for the $\Lambda_b^0 \rightarrow \Lambda_c^+ \pi^+ \pi^- \pi^-$ decays. Expectations from uncorrected and corrected (corr.) simulation are overlaid.

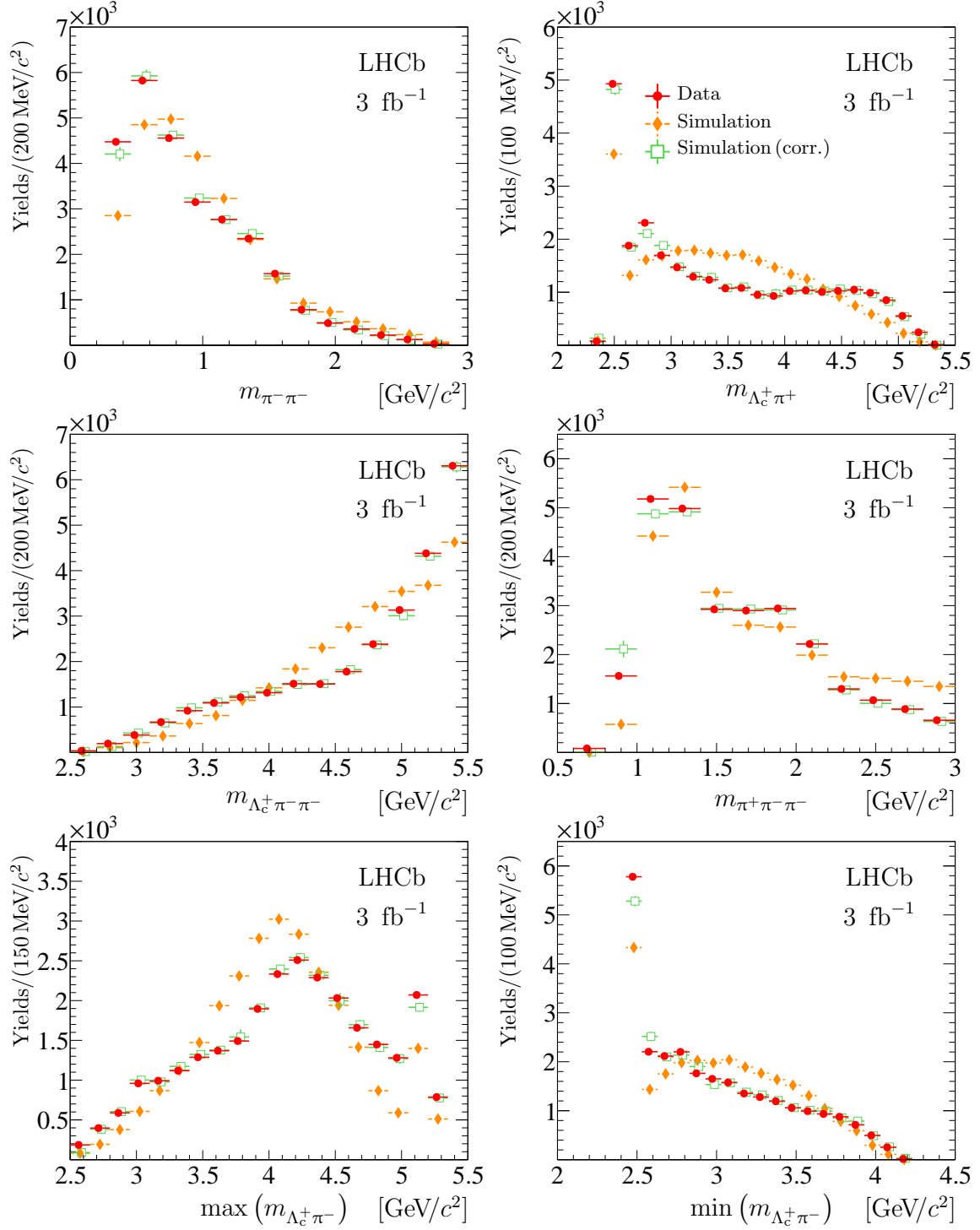


Figure A2: Background-subtracted $\pi^-\pi^-$, $\Lambda_c^+\pi^+$, $\Lambda_c^+\pi^-\pi^-$, $\Lambda_c^+\pi^+\pi^-\pi^-$, and maximum and minimum $\Lambda_c^+\pi^-$ mass spectra for the $\Lambda_b^0 \rightarrow \Lambda_c^+\pi^+\pi^-\pi^-$ decays. Expectations from uncorrected and corrected (corr.) simulation are overlaid.

References

- [1] T. Mannel and W. Roberts, *Nonleptonic Λ_b^0 decays at colliders*, Z. Phys. **C59** (1993) 179.
- [2] X. H. Guo, $\Lambda_b^0 \rightarrow \Lambda_c^+ P(V)$ *nonleptonic weak decays*, Mod. Phys. Lett. **A13** (1998) 2265, arXiv:hep-ph/9805304.
- [3] Fayyazuddin, $\Lambda_b^0 \rightarrow \Lambda D^0(\bar{D}^0)$ *decays and CP violation*, Mod. Phys. Lett. **A14** (1999) 63, arXiv:hep-ph/9806393.
- [4] A. K. Leibovich, Z. Ligeti, I. W. Stewart, and M. B. Wise, *Predictions for nonleptonic Λ_b^0 and Θ_b decays*, Phys. Lett. **B586** (2004) 337, arXiv:hep-ph/0312319.
- [5] T. Huber, S. Krankl, and X.-Q. Li, *Two-body non-leptonic heavy-to-heavy decays at NNLO in QCD factorization*, JHEP **09** (2016) 112, arXiv:1606.02888.
- [6] T. Gutsche, M. A. Ivanov, J. G. Körner, and V. E. Lyubovitskij, *Nonleptonic two-body decays of single heavy baryons Λ_Q , Ξ_Q , and Ω_Q ($Q = b, c$) induced by W emission in the covariant confined quark model*, Phys. Rev. **D98** (2018) 074011, arXiv:1806.11549.
- [7] CDF collaboration, A. Abulencia *et al.*, *Measurement of $\sigma(\Lambda_b^0)/\sigma(\bar{B}^0) \times BR(\Lambda_b^0 \rightarrow \Lambda_c^+ \pi^-)/BR(\bar{B}^0 \rightarrow D^+ \pi^-)$ in $p\bar{p}$ collisions at $\sqrt{s} = 1.96$ TeV*, Phys. Rev. Lett. **98** (2007) 122002, arXiv:hep-ex/0601003.
- [8] LHCb collaboration, R. Aaij *et al.*, *Study of the kinematic dependences of Λ_b^0 production in pp collisions and a measurement of the $\Lambda_b^0 \rightarrow \Lambda_c^+ \pi^-$ branching fraction*, JHEP **08** (2014) 143, arXiv:1405.6842.
- [9] M. Basile *et al.*, *Evidence for a new particle with naked 'beauty' and for its associated production in high-energy (pp) interactions*, Lett. Nuovo Cim. **31** (1981) 97.
- [10] G. Bari *et al.*, *The Λ_b^0 beauty baryon production in proton proton interactions at $\sqrt{s} = 62$ GeV: A second observation*, Nuovo Cim. **A104** (1991) 1787.
- [11] LHCb collaboration, R. Aaij *et al.*, *Study of beauty baryon decays to $D^0 p h^-$ and $\Lambda_c^+ h^-$ final states*, Phys. Rev. **D89** (2014) 032001, arXiv:1311.4823.
- [12] LHCb collaboration, R. Aaij *et al.*, *Study of the $D^0 p$ amplitude in $\Lambda_b^0 \rightarrow D^0 p \pi^-$ decays*, JHEP **05** (2017) 030, arXiv:1701.07873.
- [13] LHCb collaboration, R. Aaij *et al.*, *Observation of the suppressed $\Lambda_b^0 \rightarrow D p K^-$ decay with $D \rightarrow K^+ \pi^-$ and measurement of its CP asymmetry*, arXiv:2109.02621, submitted to PRD.
- [14] LHCb collaboration, A. A. Alves Jr. *et al.*, *The LHCb detector at the LHC*, JINST **3** (2008) S08005.
- [15] LHCb collaboration, R. Aaij *et al.*, *LHCb detector performance*, Int. J. Mod. Phys. **A30** (2015) 1530022, arXiv:1412.6352.

- [16] R. Aaij *et al.*, *The LHCb trigger and its performance in 2011*, JINST **8** (2013) P04022, arXiv:1211.3055.
- [17] V. V. Gligorov and M. Williams, *Efficient, reliable and fast high-level triggering using a bonsai boosted decision tree*, JINST **8** (2013) P02013, arXiv:1210.6861.
- [18] T. Sjöstrand, S. Mrenna, and P. Skands, *A brief introduction to PYTHIA 8.1*, Comput. Phys. Commun. **178** (2008) 852, arXiv:0710.3820.
- [19] I. Belyaev *et al.*, *Handling of the generation of primary events in GAUSS, the LHCb simulation framework*, J. Phys. Conf. Ser. **331** (2011) 032047.
- [20] D. J. Lange, *The EVTGEN particle decay simulation package*, Nucl. Instrum. Meth. **A462** (2001) 152.
- [21] P. Golonka and Z. Was, *PHOTOS Monte Carlo: A precision tool for QED corrections in Z and W decays*, Eur. Phys. J. **C45** (2006) 97, arXiv:hep-ph/0506026.
- [22] Geant4 collaboration, J. Allison *et al.*, *GEANT4 developments and applications*, IEEE Trans. Nucl. Sci. **53** (2006) 270; Geant4 collaboration, S. Agostinelli *et al.*, *GEANT4: A simulation toolkit*, Nucl. Instrum. Meth. **A506** (2003) 250.
- [23] M. Clemencic *et al.*, *The LHCb simulation application, GAUSS: Design, evolution and experience*, J. Phys. Conf. Ser. **331** (2011) 032023.
- [24] LHCb collaboration, R. Aaij *et al.*, *Measurement of the track reconstruction efficiency at LHCb*, JINST **10** (2015) P02007, arXiv:1408.1251.
- [25] A. Powell *et al.*, *Particle identification at LHCb*, PoS **ICHEP2010** (2010) 020, LHCb-PROC-2011-008.
- [26] M. Adinolfi *et al.*, *Performance of the LHCb RICH detector at the LHC*, Eur. Phys. J. **C73** (2013) 2431, arXiv:1211.6759.
- [27] Particle Data Group, P. A. Zyla *et al.*, *Review of particle physics*, Prog. Theor. Exp. Phys. **2020** (2020) 083C01, and 2021 update.
- [28] W. D. Hulsbergen, *Decay chain fitting with a Kalman filter*, Nucl. Instrum. Meth. **A552** (2005) 566, arXiv:physics/0503191.
- [29] T. Skwarnicki, *A study of the radiative cascade transitions between the Υ' and Υ resonances*, PhD thesis, Institute of Nuclear Physics, Krakow, 1986, DESY-F31-86-02.
- [30] LHCb collaboration, R. Aaij *et al.*, *Observation of J/ψ -pair production in pp collisions at $\sqrt{s} = 7$ TeV*, Phys. Lett. **B707** (2012) 52, arXiv:1109.0963.
- [31] M. Pivk and F. R. Le Diberder, *sPlot: A statistical tool to unfold data distributions*, Nucl. Instrum. Meth. **A555** (2005) 356, arXiv:physics/0402083.
- [32] LHCb collaboration, R. Aaij *et al.*, *Study of beauty hadron decays into pairs of charm hadrons*, Phys. Rev. Lett. **112** (2014) 202001, arXiv:1403.3606.

- [33] CLEO collaboration, F. Butler *et al.*, *Measurement of the $D^*(2010)$ branching fractions*, Phys. Rev. Lett. **69** (1992) 2041.
- [34] CLEO collaboration, J. E. Bartelt *et al.*, *Observation of the radiative decay $D^{*+} \rightarrow D^+\gamma$* , Phys. Rev. Lett. **80** (1998) 3919, arXiv:hep-ex/9711011.
- [35] E. Braaten, K.-M. Cheung, S. Fleming, and T. C. Yuan, *Perturbative QCD fragmentation functions as a model for heavy quark fragmentation*, Phys. Rev. D **51** (1995) 4819, arXiv:hep-ph/9409316.
- [36] A. F. Falk and M. E. Peskin, *Production, decay, and polarization of excited heavy hadrons*, Phys. Rev. **D49** (1994) 3320, arXiv:hep-ph/9308241.
- [37] LHCb collaboration, R. Aaij *et al.*, *Prompt charm production in pp collisions at $\sqrt{s} = 7$ TeV*, Nucl. Phys. **B871** (2013) 1, arXiv:1302.2864.
- [38] LHCb collaboration, R. Aaij *et al.*, *Measurements of prompt charm production cross-sections in pp collisions at $\sqrt{s} = 13$ TeV*, JHEP **03** (2016) 159, Erratum *ibid.* **09** (2016) 013, Erratum *ibid.* **05** (2017) 074, arXiv:1510.01707.
- [39] LHCb collaboration, R. Aaij *et al.*, *Measurements of prompt charm production cross-sections in pp collisions at $\sqrt{s} = 5$ TeV*, JHEP **06** (2017) 147, arXiv:1610.02230.
- [40] CLEO collaboration, D. Bortoletto *et al.*, *Charm production in nonresonant e^+e^- annihilations at $\sqrt{s} = 10.55$ GeV*, Phys. Rev. **D37** (1988) 1719, Erratum *ibid.* **D39** (1989) 1471.
- [41] ARGUS collaboration, H. Albrecht *et al.*, *Inclusive production of D^0 , D^+ and $D^*(2010)^+$ mesons in B decays and nonresonant e^+e^- annihilation at 10.6 GeV*, Z. Phys. **C52** (1991) 353.
- [42] ALEPH collaboration, D. Decamp *et al.*, *Production and decay of charmed mesons at the Z resonance*, Phys. Lett. **B266** (1991) 218.
- [43] VENUS collaboration, F. Hinode *et al.*, *A Study of charged D^* production in e^+e^- annihilation at an average center-of-mass energy of 58 GeV*, Phys. Lett. **B313** (1993) 245.
- [44] Belle collaboration, M. Niiyama *et al.*, *Production cross sections of hyperons and charmed baryons from e^+e^- annihilation near $\sqrt{s} = 10.52$ GeV*, Phys. Rev. **D97** (2018) 072005, arXiv:1706.06791.
- [45] ALICE collaboration, S. Acharya *et al.*, *Measurement of prompt D^0 , Λ_c^+ , and $\Sigma_c^{0,++}(2455)$ production in pp collisions at $\sqrt{s} = 13$ TeV*, arXiv:2106.08278.
- [46] R. L. Jaffe, *Exotica*, Phys. Rept. **409** (2005) 1, arXiv:hep-ph/0409065.
- [47] F. Wilczek, *Diquarks as inspiration and as objects*, in *Deserfest: A celebration of the life and works of Stanley Deser*, 322, 2004, arXiv:hep-ph/0409168.
- [48] A. Selem and F. Wilczek, *Hadron systematics and emergent diquarks*, in *Ringberg workshop on new trends in HERA Physics 2005*, 337, 2006, arXiv:hep-ph/0602128.

- [49] B. Andersson, G. Gustafson, G. Ingelman, and T. Sjöstrand, *Parton fragmentation and string dynamics*, Phys. Rept. **97** (1983) 31.

LHCb collaboration

R. Aaij³², A.S.W. Abdelmotteleb⁵⁶, C. Abellán Beteta⁵⁰, F. Abudinén⁵⁶, T. Ackernley⁶⁰, B. Adeva⁴⁶, M. Adinolfi⁵⁴, H. Afsharnia⁹, C. Agapopoulou¹³, C.A. Aidala⁸⁷, S. Aiola²⁵, Z. Ajaltouni⁹, S. Akar⁶⁵, J. Albrecht¹⁵, F. Alessio⁴⁸, M. Alexander⁵⁹, A. Alfonso Alberio⁴⁵, Z. Aliouche⁶², G. Alkhazov³⁸, P. Alvarez Cartelle⁵⁵, S. Amato², J.L. Amey⁵⁴, Y. Amhis¹¹, L. An⁴⁸, L. Anderlini²², M. Andersson⁵⁰, A. Andreianov³⁸, M. Andreotti²¹, F. Archilli¹⁷, A. Artamonov⁴⁴, M. Artuso⁶⁸, K. Arzymatov⁴², E. Aslanides¹⁰, M. Atzeni⁵⁰, B. Audurier¹², S. Bachmann¹⁷, M. Bachmayer⁴⁹, J.J. Back⁵⁶, P. Baladron Rodriguez⁴⁶, V. Balagura¹², W. Baldini²¹, J. Baptista de Souza Leite¹, M. Barbetti^{22,h}, R.J. Barlow⁶², S. Barsuk¹¹, W. Barter⁶¹, M. Bartolini⁵⁵, F. Baryshnikov⁸³, J.M. Basels¹⁴, S. Bashir³⁴, G. Bassi²⁹, B. Batsukh⁶⁸, A. Battig¹⁵, A. Bay⁴⁹, A. Beck⁵⁶, M. Becker¹⁵, F. Bedeschi²⁹, I. Bediaga¹, A. Beiter⁶⁸, V. Belavin⁴², S. Belin²⁷, V. Bellec⁵⁰, K. Belous⁴⁴, I. Belov⁴⁰, I. Belyaev⁴¹, G. Bencivenni²³, E. Ben-Haim¹³, A. Berezhnoy⁴⁰, R. Bernet⁵⁰, D. Berninghoff¹⁷, H.C. Bernstein⁶⁸, C. Bertella⁶², A. Bertolin²⁸, C. Betancourt⁵⁰, F. Betti⁴⁸, Ia. Bezshyiko⁵⁰, S. Bhasin⁵⁴, J. Bhom³⁵, L. Bian⁷³, M.S. Bieker¹⁵, N.V. Biesuz²¹, S. Bifani⁵³, P. Billoir¹³, A. Biolchini³², M. Birch⁶¹, F.C.R. Bishop⁵⁵, A. Bitadze⁶², A. Bizzeti^{22,l}, M. Bjørn⁶³, M.P. Blago⁴⁸, T. Blake⁵⁶, F. Blanc⁴⁹, S. Blusk⁶⁸, D. Bobulska⁵⁹, J.A. Boelhauve¹⁵, O. Boente Garcia⁴⁶, T. Boettcher⁶⁵, A. Boldyrev⁸², A. Bondar⁴³, N. Bondar^{38,48}, S. Borghi⁶², M. Borisyak⁴², M. Borsato¹⁷, J.T. Borsuk³⁵, S.A. Bouchiba⁴⁹, T.J.V. Bowcock^{60,48}, A. Boyer⁴⁸, C. Bozzi²¹, M.J. Bradley⁶¹, S. Braun⁶⁶, A. Brea Rodriguez⁴⁶, J. Brodzicka³⁵, A. Brossa Gonzalo⁵⁶, D. Brundu²⁷, A. Buonauro⁵⁰, L. Buonincontri²⁸, A.T. Burke⁶², C. Burr⁴⁸, A. Bursche⁷², A. Butkevich³⁹, J.S. Butter³², J. Buytaert⁴⁸, W. Byczynski⁴⁸, S. Cadeddu²⁷, H. Cai⁷³, R. Calabrese^{21,g}, L. Calefice^{15,13}, S. Cali²³, R. Calladine⁵³, M. Calvi^{26,k}, M. Calvo Gomez⁸⁵, P. Camargo Magalhaes⁵⁴, P. Campana²³, A.F. Campoverde Quezada⁶, S. Capelli^{26,k}, L. Capriotti^{20,e}, A. Carbone^{20,e}, G. Carboni^{31,q}, R. Cardinale^{24,i}, A. Cardini²⁷, I. Carli⁴, P. Carniti^{26,k}, L. Carus¹⁴, K. Carvalho Akiba³², A. Casais Vidal⁴⁶, R. Caspary¹⁷, G. Casse⁶⁰, M. Cattaneo⁴⁸, G. Cavallero⁴⁸, S. Celani⁴⁹, J. Cerasoli¹⁰, D. Cervenkov⁶³, A.J. Chadwick⁶⁰, M.G. Chapman⁵⁴, M. Charles¹³, Ph. Charpentier⁴⁸, C.A. Chavez Barajas⁶⁰, M. Chefdeville⁸, C. Chen³, S. Chen⁴, A. Chernov³⁵, V. Chobanova⁴⁶, S. Cholak⁴⁹, M. Chruszcz³⁵, A. Chubykin³⁸, V. Chulikov³⁸, P. Ciambone²³, M.F. Cicala⁵⁶, X. Cid Vidal⁴⁶, G. Ciezarek⁴⁸, P.E.L. Clarke⁵⁸, M. Clemencic⁴⁸, H.V. Cliff⁵⁵, J. Closier⁴⁸, J.L. Cobbedick⁶², V. Coco⁴⁸, J.A.B. Coelho¹¹, J. Cogan¹⁰, E. Cogneras⁹, L. Cojocariu³⁷, P. Collins⁴⁸, T. Colombo⁴⁸, L. Congedo^{19,d}, A. Contu²⁷, N. Cooke⁵³, G. Coombs⁵⁹, I. Corredoira⁴⁶, G. Corti⁴⁸, C.M. Costa Sobral⁵⁶, B. Couturier⁴⁸, D.C. Craik⁶⁴, J. Crkovská⁶⁷, M. Cruz Torres¹, R. Currie⁵⁸, C.L. Da Silva⁶⁷, S. Dadabaev⁸³, L. Dai⁷¹, E. Dall'Occo¹⁵, J. Dalseno⁴⁶, C. D'Ambrosio⁴⁸, A. Danilina⁴¹, P. d'Argent⁴⁸, A. Dashkina⁸³, J.E. Davies⁶², A. Davis⁶², O. De Aguiar Francisco⁶², K. De Bruyn⁷⁹, S. De Capua⁶², M. De Cian⁴⁹, E. De Lucia²³, J.M. De Miranda¹, L. De Paula², M. De Serio^{19,d}, D. De Simone⁵⁰, P. De Simone²³, F. De Vellis¹⁵, J.A. de Vries⁸⁰, C.T. Dean⁶⁷, F. Debernardis^{19,d}, D. Decamp⁸, V. Dedu¹⁰, L. Del Buono¹³, B. Delaney⁵⁵, H.-P. Dembinski¹⁵, A. Dendek³⁴, V. Denysenko⁵⁰, D. Derkach⁸², O. Deschamps⁹, F. Desse¹¹, F. Dettori^{27,f}, B. Dey⁷⁷, A. Di Cicco²³, P. Di Nezza²³, S. Didenko⁸³, L. Dieste Maronas⁴⁶, H. Dijkstra⁴⁸, V. Dobishuk⁵², C. Dong³, A.M. Donohoe¹⁸, F. Dordei²⁷, A.C. dos Reis¹, L. Douglas⁵⁹, A. Dovbnya⁵¹, A.G. Downes⁸, M.W. Dudek³⁵, L. Dufour⁴⁸, V. Duk⁷⁸, P. Durante⁴⁸, J.M. Durham⁶⁷, D. Dutta⁶², A. Dziurda³⁵, A. Dzyuba³⁸, S. Easo⁵⁷, U. Egede⁶⁹, V. Egorychev⁴¹, S. Eidelman^{43,v,†}, S. Eisenhardt⁵⁸, S. Ek-In⁴⁹, L. Eklund⁸⁶, S. Ely⁶⁸, A. Ene³⁷, E. Eppele⁶⁷, S. Escher¹⁴, J. Eschle⁵⁰, S. Esen⁵⁰, T. Evans⁴⁸, L.N. Falcao¹, Y. Fan⁶, B. Fang⁷³, S. Farry⁶⁰, D. Fazzini^{26,k}, M. Féo⁴⁸, A. Fernandez Prieto⁴⁶, A.D. Fernandez⁶⁶, F. Ferrari^{20,e}, L. Ferreira Lopes⁴⁹, F. Ferreira Rodrigues², S. Ferreres Sole³², M. Ferrillo⁵⁰, M. Ferro-Luzzi⁴⁸, S. Filippov³⁹, R.A. Fini¹⁹, M. Fiorini^{21,g}, M. Firlej³⁴,

K.M. Fischer⁶³, D.S. Fitzgerald⁸⁷, C. Fitzpatrick⁶², T. Fiutowski³⁴, A. Fkiaras⁴⁸, F. Fleuret¹²,
 M. Fontana¹³, F. Fontanelli^{24,i}, R. Forty⁴⁸, D. Foulds-Holt⁵⁵, V. Franco Lima⁶⁰,
 M. Franco Sevilla⁶⁶, M. Frank⁴⁸, E. Franzoso²¹, G. Frau¹⁷, C. Frei⁴⁸, D.A. Friday⁵⁹, J. Fu⁶,
 Q. Fuehring¹⁵, E. Gabriel³², G. Galati^{19,d}, A. Gallas Torreira⁴⁶, D. Galli^{20,e}, S. Gambetta^{58,48},
 Y. Gan³, M. Gandelman², P. Gandini²⁵, Y. Gao⁵, M. Garau²⁷, L.M. Garcia Martin⁵⁶,
 P. Garcia Moreno⁴⁵, J. García Pardiñas^{26,k}, B. Garcia Plana⁴⁶, F.A. Garcia Rosales¹²,
 L. Garrido⁴⁵, C. Gaspar⁴⁸, R.E. Geertsema³², D. Gerick¹⁷, L.L. Gerken¹⁵, E. Gersabeck⁶²,
 M. Gersabeck⁶², T. Gershon⁵⁶, D. Gerstel¹⁰, L. Giambastiani²⁸, V. Gibson⁵⁵, H.K. Giemza³⁶,
 A.L. Gilman⁶³, M. Giovannetti^{23,q}, A. Gioventù⁴⁶, P. Gironella Gironell⁴⁵, C. Giugliano^{21,g},
 K. Gizdov⁵⁸, E.L. Gkougkousis⁴⁸, V.V. Gligorov¹³, C. Göbel⁷⁰, E. Golobardes⁸⁵, D. Golubkov⁴¹,
 A. Golutvin^{61,83}, A. Gomes^{1,a}, S. Gomez Fernandez⁴⁵, F. Goncalves Abrantes⁶³, M. Goncerz³⁵,
 G. Gong³, P. Gorbounov⁴¹, I.V. Gorelov⁴⁰, C. Gotti²⁶, J.P. Grabowski¹⁷, T. Grammatico¹³,
 L.A. Granado Cardoso⁴⁸, E. Graugés⁴⁵, E. Graverini⁴⁹, G. Graziani²², A. Grecu³⁷,
 L.M. Greeven³², N.A. Grieser⁴, L. Grillo⁶², S. Gromov⁸³, B.R. Gruberg Cazon⁶³, C. Gu³,
 M. Guarise²¹, M. Guittiere¹¹, P. A. Günther¹⁷, A.K. Guseinov⁴¹, E. Gushchin³⁹, A. Guth¹⁴,
 Y. Guz⁴⁴, T. Gys⁴⁸, T. Hadavizadeh⁶⁹, G. Haefeli⁴⁹, C. Haen⁴⁸, J. Haimberger⁴⁸,
 T. Halewood-leagas⁶⁰, P.M. Hamilton⁶⁶, J.P. Hammerich⁶⁰, Q. Han⁷, X. Han¹⁷, T.H. Hancock⁶³,
 E.B. Hansen⁶², S. Hansmann-Menzemer¹⁷, N. Harnew⁶³, T. Harrison⁶⁰, C. Hasse⁴⁸, M. Hatch⁴⁸,
 J. He^{6,b}, M. Hecker⁶¹, K. Heijhoff³², K. Heinicke¹⁵, R.D.L. Henderson^{69,56}, A.M. Hennequin⁴⁸,
 K. Hennessy⁶⁰, L. Henry⁴⁸, J. Heuel¹⁴, A. Hicheur², D. Hill⁴⁹, M. Hilton⁶², S.E. Hollitt¹⁵,
 R. Hou⁷, Y. Hou⁸, J. Hu¹⁷, J. Hu⁷², W. Hu⁷, X. Hu³, W. Huang⁶, X. Huang⁷³,
 W. Hulsbergen³², R.J. Hunter⁵⁶, M. Hushchyn⁸², D. Hutchcroft⁶⁰, D. Hynds³², P. Ibis¹⁵,
 M. Idzik³⁴, D. Ilin³⁸, P. Ilten⁶⁵, A. Inglessi³⁸, A. Ishteev⁸³, K. Ivshin³⁸, R. Jacobsson⁴⁸,
 H. Jage¹⁴, S. Jakobsen⁴⁸, E. Jans³², B.K. Jashal⁴⁷, A. Jawahery⁶⁶, V. Jevtic¹⁵, X. Jiang⁴,
 M. John⁶³, D. Johnson⁶⁴, C.R. Jones⁵⁵, T.P. Jones⁵⁶, B. Jost⁴⁸, N. Jurik⁴⁸,
 S.H. Kalavan Kadavath³⁴, S. Kandybei⁵¹, Y. Kang³, M. Karacson⁴⁸, M. Karpov⁸²,
 J.W. Kautz⁶⁵, F. Keizer⁴⁸, D.M. Keller⁶⁸, M. Kenzie⁵⁶, T. Ketel³³, B. Khanji¹⁵, A. Kharisova⁸⁴,
 S. Kholodenko⁴⁴, T. Kirn¹⁴, V.S. Kirsebom⁴⁹, O. Kitouni⁶⁴, S. Klaver³², N. Kleijne²⁹,
 K. Klimaszewski³⁶, M.R. Kmiec³⁶, S. Koliiev⁵², A. Kondybayeva⁸³, A. Konoplyannikov⁴¹,
 P. Kopciwicz³⁴, R. Kopečna¹⁷, P. Koppenburg³², M. Korolev⁴⁰, I. Kostiuik^{32,52}, O. Kot⁵²,
 S. Kotriakhova^{21,38}, P. Kravchenko³⁸, L. Kravchuk³⁹, R.D. Krawczyk⁴⁸, M. Kreps⁵⁶, F. Kress⁶¹,
 S. Kretschmar¹⁴, P. Krokovny^{43,v}, W. Krupa³⁴, W. Krzemien³⁶, J. Kubat¹⁷, M. Kucharczyk³⁵,
 V. Kudryavtsev^{43,v}, H.S. Kuindersma^{32,33}, G.J. Kunde⁶⁷, T. Kvaratskheliya⁴¹, D. Lacarrere⁴⁸,
 G. Lafferty⁶², A. Lai²⁷, A. Lampis²⁷, D. Lancierini⁵⁰, J.J. Lane⁶², R. Lane⁵⁴, G. Lanfranchi²³,
 C. Langenbruch¹⁴, J. Langer¹⁵, O. Lantwin⁸³, T. Latham⁵⁶, F. Lazzari^{29,r}, R. Le Gac¹⁰,
 S.H. Lee⁸⁷, R. Lefèvre⁹, A. Leflat⁴⁰, S. Legotin⁸³, O. Leroy¹⁰, T. Lesiak³⁵, B. Leverington¹⁷,
 H. Li⁷², P. Li¹⁷, S. Li⁷, Y. Li⁴, Y. Li⁴, Z. Li⁶⁸, X. Liang⁶⁸, T. Lin⁶¹, R. Lindner⁴⁸,
 V. Lisovskyi¹⁵, R. Litvinov²⁷, G. Liu⁷², H. Liu⁶, Q. Liu⁶, S. Liu⁴, A. Lobo Salvia⁴⁵, A. Loi²⁷,
 J. Lomba Castro⁴⁶, I. Longstaff⁵⁹, J.H. Lopes², S. López Soliño⁴⁶, G.H. Lovell⁵⁵, Y. Lu⁴,
 C. Lucarelli^{22,h}, D. Lucchesi^{28,m}, S. Luchuk³⁹, M. Lucio Martinez³², V. Lukashenko^{32,52},
 Y. Luo³, A. Lupato⁶², E. Luppi^{21,g}, O. Lupton⁵⁶, A. Lusiani^{29,n}, X. Lyu⁶, L. Ma⁴, R. Ma⁶,
 S. Maccolini^{20,e}, F. Machefert¹¹, F. Maciuc³⁷, V. Macko⁴⁹, P. Mackowiak¹⁵,
 S. Maddrell-Mander⁵⁴, O. Madejczyk³⁴, L.R. Madhan Mohan⁵⁴, O. Maev³⁸, A. Maevskiy⁸²,
 M.W. Majewski³⁴, J.J. Malczewski³⁵, S. Malde⁶³, B. Malecki⁴⁸, A. Malinin⁸¹, T. Maltsev^{43,v},
 H. Malygina¹⁷, G. Manca^{27,f}, G. Mancinelli¹⁰, D. Manuzzi^{20,e}, D. Marangotto^{25,j}, J. Maratas^{9,t},
 J.F. Marchand⁸, U. Marconi²⁰, S. Mariani^{22,h}, C. Marin Benito⁴⁸, M. Marinangeli⁴⁹, J. Marks¹⁷,
 A.M. Marshall⁵⁴, P.J. Marshall⁶⁰, G. Martelli⁷⁸, G. Martellotti³⁰, L. Martinazzoli^{48,k},
 M. Martinelli^{26,k}, D. Martinez Santos⁴⁶, F. Martinez Vidal⁴⁷, A. Massafferri¹, M. Materok¹⁴,
 R. Matev⁴⁸, A. Mathad⁵⁰, V. Matiunin⁴¹, C. Matteuzzi²⁶, K.R. Mattioli⁸⁷, A. Mauri³²,
 E. Maurice¹², J. Mauricio⁴⁵, M. Mazurek⁴⁸, M. McCann⁶¹, L. Mcconnell¹⁸, T.H. Mcgrath⁶²,

N.T. Mchugh⁵⁹, A. McNab⁶², R. McNulty¹⁸, J.V. Mead⁶⁰, B. Meadows⁶⁵, G. Meier¹⁵,
 D. Melnychuk³⁶, S. Meloni^{26,k}, M. Merk^{32,80}, A. Merli^{25,j}, L. Meyer Garcia², M. Mikhasenko^{75,c},
 D.A. Milanese⁷⁴, E. Millard⁵⁶, M. Milovanovic⁴⁸, M.-N. Minard⁸, A. Minotti^{26,k}, L. Minzoni^{21,g},
 S.E. Mitchell⁵⁸, B. Mitreska⁶², D.S. Mitzel¹⁵, A. Mödden¹⁵, R.A. Mohammed⁶³, R.D. Moise⁶¹,
 S. Mokhnenko⁸², T. Mombächer⁴⁶, I.A. Monroy⁷⁴, S. Monteil⁹, M. Morandin²⁸, G. Morello²³,
 M.J. Morello^{29,n}, J. Moron³⁴, A.B. Morris⁷⁵, A.G. Morris⁵⁶, R. Mountain⁶⁸, H. Mu³,
 F. Muheim^{58,48}, M. Mulder⁷⁹, D. Müller⁴⁸, K. Müller⁵⁰, C.H. Murphy⁶³, D. Murray⁶²,
 R. Murta⁶¹, P. Muzzetto²⁷, P. Naik⁵⁴, T. Nakada⁴⁹, R. Nandakumar⁵⁷, T. Namut⁴⁸, I. Nasteva²,
 M. Needham⁵⁸, N. Neri^{25,j}, S. Neubert⁷⁵, N. Neufeld⁴⁸, R. Newcombe⁶¹, E.M. Niel¹¹,
 S. Nieswand¹⁴, N. Nikitin⁴⁰, N.S. Nolte⁶⁴, C. Normand⁸, C. Nunez⁸⁷, A. Oblakowska-Mucha³⁴,
 V. Obraztsov⁴⁴, T. Oeser¹⁴, D.P. O'Hanlon⁵⁴, S. Okamura²¹, R. Oldeman^{27,f}, F. Oliva⁵⁸,
 M.E. Olivares⁶⁸, C.J.G. Onderwater⁷⁹, R.H. O'Neil⁵⁸, J.M. Otalora Goicochea²,
 T. Ovsiannikova⁴¹, P. Owen⁵⁰, A. Oyanguren⁴⁷, K.O. Padeken⁷⁵, B. Pagare⁵⁶, P.R. Pais⁴⁸,
 T. Pajero⁶³, A. Palano¹⁹, M. Palutan²³, Y. Pan⁶², G. Panshin⁸⁴, A. Papanestis⁵⁷,
 M. Pappagallo^{19,d}, L.L. Pappalardo^{21,g}, C. Pappenheimer⁶⁵, W. Parker⁶⁶, C. Parkes⁶²,
 B. Passalacqua²¹, G. Passaleva²², A. Pastore¹⁹, M. Patel⁶¹, C. Patrignani^{20,e}, C.J. Pawley⁸⁰,
 A. Pearce^{48,57}, A. Pellegrino³², M. Pepe Altarelli⁴⁸, S. Perazzini²⁰, D. Pereima⁴¹,
 A. Pereiro Castro⁴⁶, P. Perret⁹, M. Petric^{59,48}, K. Petridis⁵⁴, A. Petrolini^{24,i}, A. Petrov⁸¹,
 S. Petrucci⁵⁸, M. Petruzzo²⁵, T.T.H. Pham⁶⁸, A. Philippov⁴², R. Piandani⁶, L. Pica^{29,n},
 M. Piccini⁷⁸, B. Pietrzyk⁸, G. Pietrzyk⁴⁹, M. Pili⁶³, D. Pinci³⁰, F. Pisani⁴⁸, M. Pizzichemi^{26,48,k},
 Resmi P.K¹⁰, V. Placinta³⁷, J. Plews⁵³, M. Plo Casasus⁴⁶, F. Polci¹³, M. Poli Lener²³,
 M. Poliakova⁶⁸, A. Poluektov¹⁰, N. Polukhina^{83,u}, I. Polyakov⁶⁸, E. Polycarpo², S. Ponce⁴⁸,
 D. Popov^{6,48}, S. Popov⁴², S. Poslavskii⁴⁴, K. Prasanth³⁵, L. Promberger⁴⁸, C. Prouve⁴⁶,
 V. Pugatch⁵², V. Puill¹¹, G. Punzi^{29,o}, H. Qi³, W. Qian⁶, N. Qin³, R. Quagliani⁴⁹, N.V. Raab¹⁸,
 R.I. Rabadan Trejo⁶, B. Rachwal³⁴, J.H. Rademacker⁵⁴, M. Rama²⁹, M. Ramos Pernas⁵⁶,
 M.S. Rangel², F. Ratnikov^{42,82}, G. Raven³³, M. Reboud⁸, F. Redi⁴⁹, F. Reiss⁶²,
 C. Remon Alepuz⁴⁷, Z. Ren³, V. Renaudin⁶³, R. Ribatti²⁹, A.M. Ricci²⁷, S. Ricciardi⁵⁷,
 K. Rinnert⁶⁰, P. Robbe¹¹, G. Robertson⁵⁸, A.B. Rodrigues⁴⁹, E. Rodrigues⁶⁰,
 J.A. Rodriguez Lopez⁷⁴, E.R.R. Rodriguez Rodriguez⁴⁶, A. Rollings⁶³, P. Roloff⁴⁸,
 V. Romanovskiy⁴⁴, M. Romero Lamas⁴⁶, A. Romero Vidal⁴⁶, J.D. Roth⁸⁷, M. Rotondo²³,
 M.S. Rudolph⁶⁸, T. Ruf⁴⁸, R.A. Ruiz Fernandez⁴⁶, J. Ruiz Vidal⁴⁷, A. Ryzhikov⁸², J. Ryzka³⁴,
 J.J. Saborido Silva⁴⁶, N. Sagidova³⁸, N. Sahoo⁵⁶, B. Saitta^{27,f}, M. Salomoni⁴⁸,
 C. Sanchez Gras³², R. Santacesaria³⁰, C. Santamarina Rios⁴⁶, M. Santimaria²³, E. Santovetti^{31,q},
 D. Saranin⁸³, G. Sarpis¹⁴, M. Sarpis⁷⁵, A. Sarti³⁰, C. Satriano^{30,p}, A. Satta³¹, M. Saur¹⁵,
 D. Savrina^{41,40}, H. Sazak⁹, L.G. Scantlebury Smead⁶³, A. Scarabotto¹³, S. Schael¹⁴, S. Scherl⁶⁰,
 M. Schiller⁵⁹, H. Schindler⁴⁸, M. Schmelling¹⁶, B. Schmidt⁴⁸, S. Schmitt¹⁴, O. Schneider⁴⁹,
 A. Schopper⁴⁸, M. Schubiger³², S. Schulte⁴⁹, M.H. Schune¹¹, R. Schwemmer⁴⁸, B. Sciascia^{23,48},
 S. Sellam⁴⁶, A. Semennikov⁴¹, M. Senghi Soares³³, A. Sergi^{24,i}, N. Serra⁵⁰, L. Sestini²⁸,
 A. Seuthe¹⁵, Y. Shang⁵, D.M. Shangase⁸⁷, M. Shapkin⁴⁴, I. Shchemerov⁸³, L. Shchutska⁴⁹,
 T. Shears⁶⁰, L. Shekhtman^{43,v}, Z. Shen⁵, S. Sheng⁴, V. Shevchenko⁸¹, E.B. Shields^{26,k},
 Y. Shimizu¹¹, E. Shmanin⁸³, J.D. Shupperd⁶⁸, B.G. Siddi²¹, R. Silva Coutinho⁵⁰, G. Simi²⁸,
 S. Simone^{19,d}, N. Skidmore⁶², T. Skwarnicki⁶⁸, M.W. Slater⁵³, I. Slazyk^{21,g}, J.C. Smallwood⁶³,
 J.G. Smeaton⁵⁵, A. Smetkina⁴¹, E. Smith⁵⁰, M. Smith⁶¹, A. Snoch³², L. Soares Lavra⁹,
 M.D. Sokoloff⁶⁵, F.J.P. Soler⁵⁹, A. Solovev³⁸, I. Solovyev³⁸, F.L. Souza De Almeida²,
 B. Souza De Paula², B. Spaan¹⁵, E. Spadaro Norella^{25,j}, P. Spradlin⁵⁹, F. Stagni⁴⁸, M. Stahl⁶⁵,
 S. Stahl⁴⁸, S. Stanislaus⁶³, O. Steinkamp^{50,83}, O. Stenyakin⁴⁴, H. Stevens¹⁵, S. Stone^{68,48},
 D. Strelakina⁸³, F. Suljik⁶³, J. Sun²⁷, L. Sun⁷³, Y. Sun⁶⁶, P. Svihra⁶², P.N. Swallow⁵³,
 K. Swientek³⁴, A. Szabelski³⁶, T. Szumlak³⁴, M. Szymanski⁴⁸, S. Taneja⁶², A.R. Tanner⁵⁴,
 M.D. Tat⁶³, A. Terentev⁸³, F. Teubert⁴⁸, E. Thomas⁴⁸, D.J.D. Thompson⁵³, K.A. Thomson⁶⁰,
 H. Tilquin⁶¹, V. Tisserand⁹, S. T'Jampens⁸, M. Tobin⁴, L. Tomassetti^{21,g}, X. Tong⁵,

D. Torres Machado¹, D.Y. Tou¹³, E. Trifonova⁸³, S.M. Trilov⁵⁴, C. Trippi⁴⁹, G. Tuci⁶, A. Tully⁴⁹, N. Tuning^{32,48}, A. Ukleja^{36,48}, D.J. Unverzagt¹⁷, E. Ursov⁸³, A. Usachov³², A. Ustyuzhanin^{42,82}, U. Uwer¹⁷, A. Vagner⁸⁴, V. Vagnoni²⁰, A. Valassi⁴⁸, G. Valenti²⁰, N. Valls Canudas⁸⁵, M. van Beuzekom³², M. Van Dijk⁴⁹, H. Van Hecke⁶⁷, E. van Herwijnen⁸³, M. van Veghel⁷⁹, R. Vazquez Gomez⁴⁵, P. Vazquez Regueiro⁴⁶, C. Vázquez Sierra⁴⁸, S. Vecchi²¹, J.J. Velthuis⁵⁴, M. Veltri^{22,s}, A. Venkateswaran⁶⁸, M. Veronesi³², M. Vesterinen⁵⁶, D. Vieira⁶⁵, M. Vieites Diaz⁴⁹, H. Viemann⁷⁶, X. Vilasis-Cardona⁸⁵, E. Vilella Figueras⁶⁰, A. Villa²⁰, P. Vincent¹³, F.C. Volle¹¹, D. Vom Bruch¹⁰, A. Vorobyev³⁸, V. Vorobyev^{43,v}, N. Voropaev³⁸, K. Vos⁸⁰, R. Waldi¹⁷, J. Walsh²⁹, C. Wang¹⁷, J. Wang⁵, J. Wang⁴, J. Wang³, J. Wang⁷³, M. Wang³, R. Wang⁵⁴, Y. Wang⁷, Z. Wang⁵⁰, Z. Wang³, Z. Wang⁶, J.A. Ward^{56,69}, N.K. Watson⁵³, S.G. Weber¹³, D. Websdale⁶¹, C. Weisser⁶⁴, B.D.C. Westhenry⁵⁴, D.J. White⁶², M. Whitehead⁵⁴, A.R. Wiederhold⁵⁶, D. Wiedner¹⁵, G. Wilkinson⁶³, M. Wilkinson⁶⁸, I. Williams⁵⁵, M. Williams⁶⁴, M.R.J. Williams⁵⁸, F.F. Wilson⁵⁷, W. Wislicki³⁶, M. Witek³⁵, L. Witola¹⁷, G. Wormser¹¹, S.A. Wotton⁵⁵, H. Wu⁶⁸, K. Wyllie⁴⁸, Z. Xiang⁶, D. Xiao⁷, Y. Xie⁷, A. Xu⁵, J. Xu⁶, L. Xu³, M. Xu⁵⁶, Q. Xu⁶, Z. Xu⁹, Z. Xu⁶, D. Yang³, S. Yang⁶, Y. Yang⁶, Z. Yang⁵, Z. Yang⁶⁶, Y. Yao⁶⁸, L.E. Yeomans⁶⁰, H. Yin⁷, J. Yu⁷¹, X. Yuan⁶⁸, O. Yushchenko⁴⁴, E. Zaffaroni⁴⁹, M. Zavertyaev^{16,u}, M. Zdybal³⁵, O. Zenaiev⁴⁸, M. Zeng³, D. Zhang⁷, L. Zhang³, S. Zhang⁷¹, S. Zhang⁵, Y. Zhang⁵, Y. Zhang⁶³, A. Zharkova⁸³, A. Zhelezov¹⁷, Y. Zheng⁶, T. Zhou⁵, X. Zhou⁶, Y. Zhou⁶, V. Zhovkovska¹¹, X. Zhu³, X. Zhu⁷, Z. Zhu⁶, V. Zhukov^{14,40}, J.B. Zonneveld⁵⁸, Q. Zou⁴, S. Zucchelli^{20,e}, D. Zuliani²⁸, G. Zunica⁶².

¹Centro Brasileiro de Pesquisas Físicas (CBPF), Rio de Janeiro, Brazil

²Universidade Federal do Rio de Janeiro (UFRJ), Rio de Janeiro, Brazil

³Center for High Energy Physics, Tsinghua University, Beijing, China

⁴Institute Of High Energy Physics (IHEP), Beijing, China

⁵School of Physics State Key Laboratory of Nuclear Physics and Technology, Peking University, Beijing, China

⁶University of Chinese Academy of Sciences, Beijing, China

⁷Institute of Particle Physics, Central China Normal University, Wuhan, Hubei, China

⁸Univ. Savoie Mont Blanc, CNRS, IN2P3-LAPP, Annecy, France

⁹Université Clermont Auvergne, CNRS/IN2P3, LPC, Clermont-Ferrand, France

¹⁰Aix Marseille Univ, CNRS/IN2P3, CPPM, Marseille, France

¹¹Université Paris-Saclay, CNRS/IN2P3, IJCLab, Orsay, France

¹²Laboratoire Leprince-Ringuet, CNRS/IN2P3, Ecole Polytechnique, Institut Polytechnique de Paris, Palaiseau, France

¹³LPNHE, Sorbonne Université, Paris Diderot Sorbonne Paris Cité, CNRS/IN2P3, Paris, France

¹⁴I. Physikalisches Institut, RWTH Aachen University, Aachen, Germany

¹⁵Fakultät Physik, Technische Universität Dortmund, Dortmund, Germany

¹⁶Max-Planck-Institut für Kernphysik (MPIK), Heidelberg, Germany

¹⁷Physikalisches Institut, Ruprecht-Karls-Universität Heidelberg, Heidelberg, Germany

¹⁸School of Physics, University College Dublin, Dublin, Ireland

¹⁹INFN Sezione di Bari, Bari, Italy

²⁰INFN Sezione di Bologna, Bologna, Italy

²¹INFN Sezione di Ferrara, Ferrara, Italy

²²INFN Sezione di Firenze, Firenze, Italy

²³INFN Laboratori Nazionali di Frascati, Frascati, Italy

²⁴INFN Sezione di Genova, Genova, Italy

²⁵INFN Sezione di Milano, Milano, Italy

²⁶INFN Sezione di Milano-Bicocca, Milano, Italy

²⁷INFN Sezione di Cagliari, Monserrato, Italy

²⁸Università degli Studi di Padova, Università e INFN, Padova, Padova, Italy

²⁹INFN Sezione di Pisa, Pisa, Italy

³⁰INFN Sezione di Roma La Sapienza, Roma, Italy

³¹INFN Sezione di Roma Tor Vergata, Roma, Italy

- ³² *Nikhef National Institute for Subatomic Physics, Amsterdam, Netherlands*
- ³³ *Nikhef National Institute for Subatomic Physics and VU University Amsterdam, Amsterdam, Netherlands*
- ³⁴ *AGH - University of Science and Technology, Faculty of Physics and Applied Computer Science, Kraków, Poland*
- ³⁵ *Henryk Niewodniczanski Institute of Nuclear Physics Polish Academy of Sciences, Kraków, Poland*
- ³⁶ *National Center for Nuclear Research (NCBJ), Warsaw, Poland*
- ³⁷ *Horia Hulubei National Institute of Physics and Nuclear Engineering, Bucharest-Magurele, Romania*
- ³⁸ *Petersburg Nuclear Physics Institute NRC Kurchatov Institute (PNPI NRC KI), Gatchina, Russia*
- ³⁹ *Institute for Nuclear Research of the Russian Academy of Sciences (INR RAS), Moscow, Russia*
- ⁴⁰ *Institute of Nuclear Physics, Moscow State University (SINP MSU), Moscow, Russia*
- ⁴¹ *Institute of Theoretical and Experimental Physics NRC Kurchatov Institute (ITEP NRC KI), Moscow, Russia*
- ⁴² *Yandex School of Data Analysis, Moscow, Russia*
- ⁴³ *Budker Institute of Nuclear Physics (SB RAS), Novosibirsk, Russia*
- ⁴⁴ *Institute for High Energy Physics NRC Kurchatov Institute (IHEP NRC KI), Protvino, Russia, Protvino, Russia*
- ⁴⁵ *ICCUB, Universitat de Barcelona, Barcelona, Spain*
- ⁴⁶ *Instituto Galego de Física de Altas Enerxías (IGFAE), Universidade de Santiago de Compostela, Santiago de Compostela, Spain*
- ⁴⁷ *Instituto de Física Corpuscular, Centro Mixto Universidad de Valencia - CSIC, Valencia, Spain*
- ⁴⁸ *European Organization for Nuclear Research (CERN), Geneva, Switzerland*
- ⁴⁹ *Institute of Physics, Ecole Polytechnique Fédérale de Lausanne (EPFL), Lausanne, Switzerland*
- ⁵⁰ *Physik-Institut, Universität Zürich, Zürich, Switzerland*
- ⁵¹ *NSC Kharkiv Institute of Physics and Technology (NSC KIPT), Kharkiv, Ukraine*
- ⁵² *Institute for Nuclear Research of the National Academy of Sciences (KINR), Kyiv, Ukraine*
- ⁵³ *University of Birmingham, Birmingham, United Kingdom*
- ⁵⁴ *H.H. Wills Physics Laboratory, University of Bristol, Bristol, United Kingdom*
- ⁵⁵ *Cavendish Laboratory, University of Cambridge, Cambridge, United Kingdom*
- ⁵⁶ *Department of Physics, University of Warwick, Coventry, United Kingdom*
- ⁵⁷ *STFC Rutherford Appleton Laboratory, Didcot, United Kingdom*
- ⁵⁸ *School of Physics and Astronomy, University of Edinburgh, Edinburgh, United Kingdom*
- ⁵⁹ *School of Physics and Astronomy, University of Glasgow, Glasgow, United Kingdom*
- ⁶⁰ *Oliver Lodge Laboratory, University of Liverpool, Liverpool, United Kingdom*
- ⁶¹ *Imperial College London, London, United Kingdom*
- ⁶² *Department of Physics and Astronomy, University of Manchester, Manchester, United Kingdom*
- ⁶³ *Department of Physics, University of Oxford, Oxford, United Kingdom*
- ⁶⁴ *Massachusetts Institute of Technology, Cambridge, MA, United States*
- ⁶⁵ *University of Cincinnati, Cincinnati, OH, United States*
- ⁶⁶ *University of Maryland, College Park, MD, United States*
- ⁶⁷ *Los Alamos National Laboratory (LANL), Los Alamos, United States*
- ⁶⁸ *Syracuse University, Syracuse, NY, United States*
- ⁶⁹ *School of Physics and Astronomy, Monash University, Melbourne, Australia, associated to ⁵⁶*
- ⁷⁰ *Pontifícia Universidade Católica do Rio de Janeiro (PUC-Rio), Rio de Janeiro, Brazil, associated to ²*
- ⁷¹ *Physics and Micro Electronic College, Hunan University, Changsha City, China, associated to ⁷*
- ⁷² *Guangdong Provincial Key Laboratory of Nuclear Science, Guangdong-Hong Kong Joint Laboratory of Quantum Matter, Institute of Quantum Matter, South China Normal University, Guangzhou, China, associated to ³*
- ⁷³ *School of Physics and Technology, Wuhan University, Wuhan, China, associated to ³*
- ⁷⁴ *Departamento de Física, Universidad Nacional de Colombia, Bogota, Colombia, associated to ¹³*
- ⁷⁵ *Universität Bonn - Helmholtz-Institut für Strahlen und Kernphysik, Bonn, Germany, associated to ¹⁷*
- ⁷⁶ *Institut für Physik, Universität Rostock, Rostock, Germany, associated to ¹⁷*
- ⁷⁷ *Eotvos Lorand University, Budapest, Hungary, associated to ⁴⁸*
- ⁷⁸ *INFN Sezione di Perugia, Perugia, Italy, associated to ²¹*
- ⁷⁹ *Van Swinderen Institute, University of Groningen, Groningen, Netherlands, associated to ³²*
- ⁸⁰ *Universiteit Maastricht, Maastricht, Netherlands, associated to ³²*

- ⁸¹ *National Research Centre Kurchatov Institute, Moscow, Russia, associated to* ⁴¹
⁸² *National Research University Higher School of Economics, Moscow, Russia, associated to* ⁴²
⁸³ *National University of Science and Technology “MISIS”, Moscow, Russia, associated to* ⁴¹
⁸⁴ *National Research Tomsk Polytechnic University, Tomsk, Russia, associated to* ⁴¹
⁸⁵ *DS4DS, La Salle, Universitat Ramon Llull, Barcelona, Spain, associated to* ⁴⁵
⁸⁶ *Department of Physics and Astronomy, Uppsala University, Uppsala, Sweden, associated to* ⁵⁹
⁸⁷ *University of Michigan, Ann Arbor, United States, associated to* ⁶⁸

^a *Universidade Federal do Triângulo Mineiro (UFTM), Uberaba-MG, Brazil*

^b *Hangzhou Institute for Advanced Study, UCAS, Hangzhou, China*

^c *Excellence Cluster ORIGINS, Munich, Germany*

^d *Università di Bari, Bari, Italy*

^e *Università di Bologna, Bologna, Italy*

^f *Università di Cagliari, Cagliari, Italy*

^g *Università di Ferrara, Ferrara, Italy*

^h *Università di Firenze, Firenze, Italy*

ⁱ *Università di Genova, Genova, Italy*

^j *Università degli Studi di Milano, Milano, Italy*

^k *Università di Milano Bicocca, Milano, Italy*

^l *Università di Modena e Reggio Emilia, Modena, Italy*

^m *Università di Padova, Padova, Italy*

ⁿ *Scuola Normale Superiore, Pisa, Italy*

^o *Università di Pisa, Pisa, Italy*

^p *Università della Basilicata, Potenza, Italy*

^q *Università di Roma Tor Vergata, Roma, Italy*

^r *Università di Siena, Siena, Italy*

^s *Università di Urbino, Urbino, Italy*

^t *MSU - Iligan Institute of Technology (MSU-IIT), Iligan, Philippines*

^u *P.N. Lebedev Physical Institute, Russian Academy of Science (LPI RAS), Moscow, Russia*

^v *Novosibirsk State University, Novosibirsk, Russia*

[†] *Deceased*